Article:
Mohammed-Sajed, OK and Glover, PWJ orcid.org/0000-0003-1715-5474 (2022) Influence of anhydritisation on the reservoir quality of the Butmah Formation in north-western Iraq. Marine and Petroleum Geology, 135. 105391. ISSN 0264-8172

https://doi.org/10.1016/j.marpetgeo.2021.105391

Influence of anhydritisation on the reservoir quality of the Butmah Formation in north-western Iraq

Omar K. Mohammed-Sajed[a,b] and Paul W.J. Glover[b]

[a]*Department of Geology, College of Science, University of Mosul, Iraq*

[b]*School of Earth and Environment, University of Leeds, UK.*

Abstract. Carbonates and evaporites in the Butmah Formation (Lower Jurassic) were deposited in restricted marine (inner ramp) environments in north-western Iraq. The carbonates are composed of ooidal, peloidal and fossiliferous limestone in shoal and lagoon facies, while syndepositional dolomite with early anhydrite cement is found in tidal flat facies. Study of anhydrite intervals shows different structures represented by bedded, massive, chicken-wire and nodular structures which consist petrographically of fibrous, equant, felted, spare crystal, needle and lath shape textures. Two phases of anhydrite cementation were recognised in this study: Phase I is represented by syndepositional anhydrite cement that affected the reservoir quality of the tidal flat facies, and Phase II as late anhydrite cement that affected the reservoir quality of the lagoon and shoal facies. Extensive petrophysical measurements were carried out and have shown that differences in lithology, anhydrite cement type, and the degree of anhydritisation control the reservoir quality of the Butmah Formation. The Butmah Formation was divided into three rock types according to differences in their petrophysical properties and the anhydrite cement fraction. Quantitative and qualitative observations combine to indicate that post-depositional uplift may have affected the study area during the Middle-Late Jurassic and tended to dissolve some of the anhydrite cement in the tidal flat facies, creating sulfate-rich brines, and then movement of those brines toward the lagoon and shoal facies led to saturation and deposition as late anhydrite cementation (Phase II). This mechanism has affected the reservoir quality of the Butmah Formation considerably, altering its petrophysical properties.

Keywords: Anhydritisation, reservoir quality, anhydrite textures, Butmah Formation, inner platform, porosity, permeability, cementation exponent

1. INTRODUCTION

Anhydrite plays an active role in many recently discovered hydrocarbon prospects, which generally consist of anhydrite-rich carbonate successions, and where anhydrite also acts as trap seals which are controlled by the stratigraphic distribution of anhydrite-carbonate facies (Sarg, 2001; El-Tabakh et al., 2004; Warren, 2010; Esrafili-Dizaji and Rahimpour-Bonab, 2009; Rahimpour-Bonab et al., 2010; Tavakoli et al., 2011; Aleali et al., 2013; Amel et al., 2015).

Anhydrite usually occurs interbedded with carbonates, and is an indicator of dry periods and shallow depositional environments (Warren, 2010). There are many such formations in the Middle East, such as the Dalan and Kangan formations in Iran and the Khuff Formation in Oman (Alsharhan, 2006; Maurer et al., 2009; Esrafili-Dizaji and Rahimpour-Bonab, 2009; Koehrer et al., 2010; Rahimpour-Bonab et al., 2010; Tavakoli et al., 2011; Aleali et al., 2013; Amel et al., 2015). The Butmah Formation (Lower Jurassic), studied in this paper, represents one of the best examples of anhydritised carbonate in Iraq (Aqrawi et al., 2010).

Anhydrite fabrics, including structures, depositional textures, and diagenetic features, have affected widely the reservoir quality of the Butmah Formation (Aqrawi et al., 2010). Usually, anhydrite cement has a negative influence on reservoir quality by occluding pores and fractures (Mohammed Sajed and Glover, 2020). However, a few studies have reported that anhydrite components can be present in significant amounts while not affecting the overall reservoir quality, and in some cases even improve reservoir quality if the formation has been subjected to uplift or late dissolution (Lucia and Ruppel, 1996; Lucia, 1999; Lucia, 2004).

The influence of anhydrite on the reservoir quality of carbonate rocks has been studied in a number of major Middle-Eastern hydrocarbon reservoirs, such as the early Triassic Kangan Formation (Esrafili-Dizaji and Rahimpour-Bonab, 2009; Rahimpour-Bonab et al., 2010;

Tavakoli et al., 2011; Aleali et al., 2013), the Permian Khuff and Dalan formations (Alsharhan, 2006; Ehrenberg, 2006; Ehrenberg et al., 2007; Maurer et al., 2009; Esrafili-Dizaji and Rahimpour-Bonab, 2009; Koehrer et al., 2010; Rahimpour-Bonab et al., 2010; Tavakoli et al., 2011; Amel et al., 2015), and the Jurassic Butmah Formation (Mohammed Sajed and Glover, 2020; Mohammed Sajed et al., 2021). However, little research has addressed the control exhibited by different degrees and styles of anhydritisation on porosity-permeability relationships (Warren, 2006; Lucia et al., 2004). Moreover, only a few studies have characterised the Butmah Formation in Iraq (Bellen et al., 1959; Ahmad, 1997; Jassim et al., 2006; Aqrawi et al., 2010).

Consequently, this paper represents the first study to examine the anhydrite fabrics of the Butmah Formation divides the formation into three rock types according to anhydrite fabric and petrophysical properties. This paper also attempts to identify relationships between anhydrite fabrics and a range of petrophysical properties (e.g., porosity, permeability, and pore throat size) so that such relationships can be compared with those from other carbonate successions or used as a reference.

This paper has three aims. The first is to provide enhanced data, analysis and discussion concerning the carbonate lithofacies of the Butmah formation. The second aim is to examine the positive and negative effects of the amount and texture of anhydrite fabrics on the reservoir quality of the Butmah Formation, with a view to understanding the diagenetic effect and tectonic mechanism that created the final shape of the pore network. The last aim is to understand the control that anhydrite has on the porosity-hydraulic permeability (poroperm) and porosity-electrical connectedness (poroconn) relationships, and through them, on the reservoir quality of the formation.

2. THE BUTMAH FORMATION

2.1. Geological setting

The study area is located in north-western Iraq, where the Butmah Formation occurs within the Ain Zalah and Butmah anticlines. The Ain Zalah anticline is a doubly plunging anticline, located within the Zagros foothills zone, about 60 km northwest of Mosul city in northern Iraq (Dunnington, 1958; Foad, 2015; Mohammed Sajed and Glover, 2020). It is about 20 km long by 5 km wide and has an elevation of 457 m above sea level (Dunnington, 1958; Hart and Hay, 1974).

The Butmah anticline is located about 10 km south-east of and parallel to the Ain Zalah anticline in northern Iraq (Figure 1A). It is an asymmetrical anticline consisting of two domes, eastern and western, and is about 12 km long and 6 km wide. The main oil-producing formations are the fractured limestones of the Shiranish Formation (Campanian- Lower Maastrichtian) and the dolomitised carbonates of the Mauddud Formation (Albian) in both anticlines. There is also minor oil production in some wells from the Butmah Formation (Lower Jurassic) and Kurrachine Formation (Upper Triassic) (Aqrawi et al., 2010; Mohammed Sajed et al., 2021).

There is no outcrop of the Butmah Formation in Iraq. However, it is penetrated by wells with a thickness of 162-500 m in north-western Iraq (Bellen et al., 1959; Jasim et al., 2006). The type section of the Butmah Formation was described by Dunnington in 1953 (Bellen et al., 1959) from the well 'Butmah-2' in the Low Folded Zone of northern Iraq as a 500 m thick heterogeneous carbonate unit.

The thickness of the formation in the wells within the study area is constrained by the wells 'Butmah-15' (402 m) and 'Ain Zalah-29' (473m), the latter of which represents the greatest logged thickness of the formation in north-western Iraq (Mohammed Sajed and Glover 2020). Figure 1 shows the position of the Butmah Formation within north-western Iraq and a summary of the main stratigraphic units based on a log from well Bm-15.

2.2. Stratigraphy

The type section of the Butmah Formation in the well 'Butmah-2' is divided into three parts (Figure 1B). The lower part, approximately 120 m thick, consists of limestone interbedded with anhydrite. This is overlain by about 180 m of oolitic and pseudo-oolitic, argillaceous and dolomitic limestone, with sandstone and shale beds. The upper part is about 200 m thick and is composed of oolitic, pseudo-oolitic and detrital limestones with argillaceous limestone, shale and anhydrite (Jasim et al., 2006).

Mohammed Sajed and Glover (2020) and Mohammed Sajed et al. (2021) characterised the Butmah Formation at the Ain Zalah and Butmah oilfields by three main lithofacies:

1. Lithofacies-1 consists of microcrystalline limestone, with or without anhydrite nodules, and is repeated three times as units 1, 3, and 5.
2. Lithofacies-2 is composed of dolomite interbedded with shale and some anhydrite nodules. It is represented as Unit 2 of the Butmah Formation in well Bm-15, and represents about 17.8% of the total thickness at this location.
3. Lithofacies-3 is composed of dolomite with anhydrite nodules and is interbedded with anhydrite layers. It is found in Unit 4, and is the most common lithofacies in the studied well (Bm-15), representing 53.4% of the gross thickness of the Butmah Formation at that location.

Figure 1B shows the stratigraphy in well Bm-15 as defined by Mohammed Sajed and Glover (2020) and Mohammed Sajed and Glover (2021) with the relationships between the units and lithofacies and the gamma ray log.

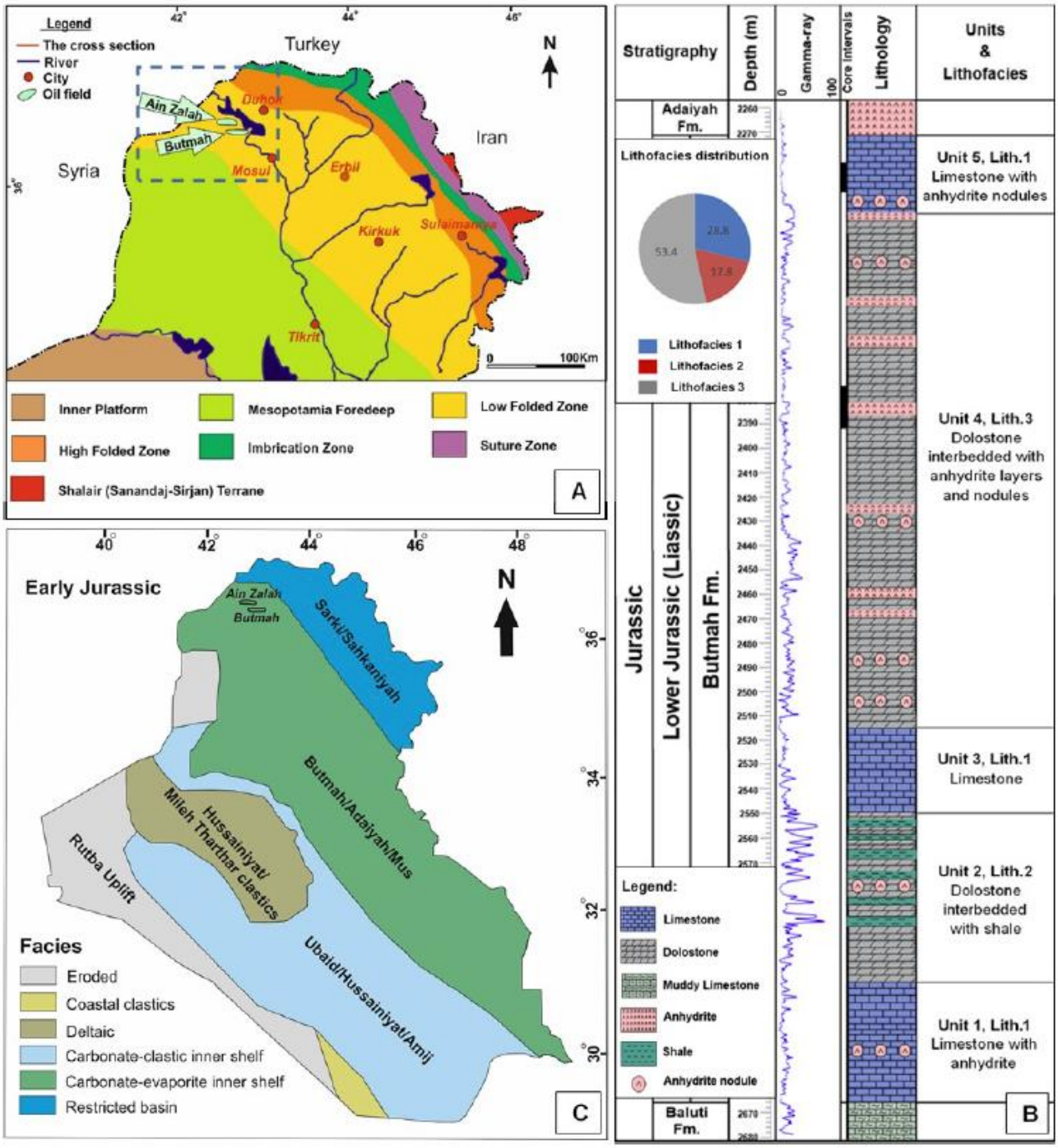

Figure 1. (A) The location of the Ain Zalah and Butmah oilfield in north-western Iraq with the tectonic division of Iraq (after Fouad, 2015); (B) Stratigraphic units of the Butmah Formation at well Bm-15. The term 'lithofacies' was used to identify the lithology, whereas 'stratigraphic unit (unit)' was used to characterise the vertical distribution of the lithofacies in succession (after Mohammed Sajed and Glover, 2020; Mohammed Sajed et al., 2021); (C) The location of the Ain-Zalah and Butmah oilfields in north-western Iraq concerning the palaeography of the late Liassic (after Jassim et al., 2006).

2.3. Tectonism and Palaeogeography

The Butmah Formation was deposited during the Liassic sequence (Lower Jurassic) of the late Permian-Liassic megasequence (AP6) of Sharland et al. (2001). Tectonically, the study area suffered from extension at the northern and eastern margins of the Arabian plate in the Middle-Late Triassic, which caused rifting followed by slow thermal subsidence in the Norian-Liassic (Lower Jurassic) sequence. As a result, the Mesopotamian Basin post-rift infill was composed of uniform marginal marine clastics, evaporites and shallow lagoonal carbonates. The Middle-Late Jurassic sequence in northern Iraq was deposited at the time of the separation of the Mesopotamian Intra-shelf Basin from the Neo-Tethyan Ocean, which can probably be attributed to the renewed rifting along the north-east margin of the Arabian Plate (Jasim and Goff, 2006; Aqrawi et al., 2010).

The Liassic sequence is composed of nine formations, as shown in Figure 1C. The clastic carbonate inner shelf in western Iraq is represented by the Ubaid, Hussainiyat and Amij formations, while the Butmah, Adaiyah, Alan and Mus formations make up the carbonate-evaporite inner shelf in central Iraq and the Low Folded Zone. The Sarki and Sehkaniyan Formations comprise restricted lagoonal carbonates in the High Folded and Balambo-Tanjero Zones in northern and northeastern Iraq (Jasim et al., 2006).

3. METHODOLOGY

3.1 Pore and grain structure micrography

A total of 652 thin section slides from cores and chippings from the Butmah Formation in wells Bm-15, and Az-29 have been studied. All the thin section slides were prepared using a blue-dyed epoxy so that the pore spaces were easier to identify, classify and measure. Dickson's (1965) staining technique was used to differentiate between calcite, ferroan calcite, and dolomite minerals. This technique employs a mixture of hydrochloric acid (HCl), alizarin red (1,2-dihydroxyanthraquinone; $C_{14}H_8O_4$) and potassium ferricyanide ($K_3[Fe(CN)_6]$).

In addition, a subset of 16 samples were chosen for identifying pores at nanometric scale using scanning electron microscopy (SEM). Examples from both limestone and dolomite units were selected according to their limestone/dolomite texture, the type and amount of different anhydrite fabrics, and their porosity-permeability (poroperm) relationship. Each sample took the form of an approximate cuboid with a nominal side length of 7 mm, and both broken and polished surfaces. The samples were glued onto aluminium stubs and then coated with a conducting carbon film to be ready for digital recording of the SEM images (Erdman and Bell, 2015). The samples were imaged using magnifications of 1:500 to 1:10,000 in both back-scattered and secondary electron imaging modes. ImageJ® software (ver. 1.53e) was used for analysing the captured images.

3.2 Porosity and permeability

A set of 67 core plug samples was provided by the North Oil Company from the core intervals within the studied wells. Each of these cylindrical core plugs was nominally 1.5 inches in diameter and 2 inches in length. They were cleaned using Soxhlet extraction and dried in a temperature controlled oven at 60°C for 48 h. The porosity of the dried samples was measured using helium pycnometry at a pressure ≤15 psig (Spain, 1992; McPhee et al., 2015). The measurements were carried out using the apparatus and protocols of the Wolfson laboratory at the University of Leeds. The porosity measurement for each core plug sample was repeated three times, with arithmetic mean values and range given in this paper.

Klinkenberg permeability was measured with a pulse-decay permeameter (k ≤ 1 mD) (Jones, 1997; Jannot et al., 2007; Zhang et al., 2000; Tiab and Donaldson, 2012; McPhee et al., 2015) using helium gas with confining pressure of 4500 psig, in the Wolfson laboratory at the University of Leeds. The measured samples were tested at effective stresses of 900 psig and at pore fluid pressures of 750, 600, 450, and 300 psig. The raw experimental measurements were corrected for so-called gas ‘slippage’ which occurs when the requirement for continuity in the gas breaks down (Klinkenberg, 1941; Rushing et al., 2004; Haines et al., 2016). It is extremely important to make this correction for tight rocks because the small size of the pore

and pore-throat microstructure exacerbates the problem of gas slippage (Rashid et al., 2017; Mohammed Sajed and Glover, 2020).

3.3 Pore throat measurements

Mercury injection capillary pressure (MICP) tests were used in this study to derive pore-throat size distributions (Jennings, 1987; Kopaska-Merkel and Amthor, 1988; Katz and Thompson, 1987; Glover et al., 2006) using the Young-Laplace equation (Washburn, 1921). Eight samples were selected for MICP testing according to their lithology, porosity, and permeability. The samples were cut to dimensions of approximately 15 mm to 10 mm, cleaned, and evacuated. Mercury intrusion data were obtained using a Micromeritics Autopore IV 9250 apparatus and pressure up to 60,000 psig (Giesche, 2006). Pore size distributions were obtained from the pore-throat size distributions using the Glover and Dery (2010) method, and the Glover and Walker (2009) method was then used to derive the grain/crystal size distributions.

3.4 Electrical resistivity and cementation exponent

Electrical resistivity measurements were carried out on the same 67 core plugs as had been previously measured for porosity and permeability. They were prepared by placing them in a vacuum desiccator, followed by full saturation with the synthetic formation water for 24 hours. The samples were then loaded into a high-pressure saturation core holder filled with the same synthetic formation brine and left for 48 hours under a pressure of 100 psig. The synthetic formation brine was prepared based on the composition of the formation brine in the final well report of the studied wells. It is composed of 0.602 (g/dm^3) $Ca(HCO_3)_2$, 37.50 (g/dm^3) $CaCl_2$, 7.29 (g/dm^3) $MgCl_2$, and 94.982 (g/dm^3) NaCl. This synthetic brine has a NaCl equivalent salinity of 151.69 g/dm^3, which is highly saline. The brine has a theoretical electrical conductivity of 16.75 S/m at 25°C according to the method of Sen and Goode (1992a; b).

The conductivity of the formation brine was measured at the Wolfson laboratory temperature, and found to be 0.02±0.01 S/m at 22.3°C. The brine conductivity was then converted to resistivity and corrected to reservoir temperature using Arp's formula (Asquith and Krygowski,

2004). The formation factor of each sample was calculated from the measured electrical resistivity, and the cementation exponent for each sample was calculated using standard equations linking the cementation exponent, formation factor and porosity (Glover, 2015).

4. ANHYDRITE FABRICS

The term 'fabric' is used to describe qualitatively the complete spatial arrangement of all components in a rock including both texture and structure (Passchier and Throuw, 2005). The interpretation of geological, geophysical and geochemical processes leading to different anhydrite fabrics (including sedimentary structures and petrographic textures) provides a key to unlocking the palaeoenvironment and palaeoclimate mystery which ultimately provides vital information about the sea-level fluctuations, salinity, depth, and temperature (Kendall, 1984; Tucker, 1991; Warren, 2006). According to the Mohammed Sajed and Glover (2020) and Mohammed Sajed et al. (2021), the Butmah Formation consists of three main lithofacies (Figure 1b) and these lithofacies contain different types of anhydrite fabrics (structures and textures). In this section we review the structures and textures observed in the characterised lithofacies of the Butmah Formation.

4.1 Anhydrite structures

At least five different kinds of anhydrite structure at core-scale have been recognised in the Butmah Formation, as summarised below.

4.1.1 Nodular anhydrite and chicken-wire structures

Anhydrite nodules are characterised by irregularly shaped lumps (oval, spherical and lenticular) of anhydrite with a diameter range of 0.4 mm - 5 cm, white to milky in colour, and distributed in both limestone and dolomite lithofacies of the studied formation. In most cases, these nodules are aggregated to form irregular anhydrite layers separated by very thin films of mudstone and dolomudstone remnants, creating a chicken-wire texture, which can be seen

in Figure 2. Under microscopic study these structures appear to consist of mosaic to fibrous and/or equant anhydrite crystals.

4.1.2 Bedded or laminated anhydrite structures

Bedded or laminated anhydrite structures consist of sub-horizontal layers or beds of dense crystalline anhydrite a few millimetres to a few centimetres in thickness, with the term 'bedded' applying to the thicker layers, and with the term 'laminated' referring to successions of finer layers. Beds or layers are white to grey in colour and may have a planar or irregular morphology (Figure 2).

4.1.3 Massive anhydrite structures

Massive anhydrite is composed of white to brown crystalline anhydrite with a thickness from a few centimetres to 0.5 m, as shown in Figure 2. In thin section, massive anhydrite shows a variety of textures including equant, felted, fibrous and bladed. In the Butmah Formation massive anhydrite structures are less common than the other types of structure.

4.2 Petrographic anhydrite textures

Six types of small-scale anhydrite textures were observed in the Butmah Formation using various types of micrography, and these are summarised below.

4.2.1 Aphanitic and felted textures

When viewed in thin section under crossed polarisers, the aphanitic texture consists of very fine crystals (less than 5 μm) which exhibit random orientations that may be locally aligned, leading to random or locally patchy birefringence that gives the texture a colourful aspect, as shown in Figure 3A. By contrast, the felted texture (Figure 3B) is composed of larger (between 5-100 μm long and 5-20 μm wide), closely packed and well aligned crystals, and sometimes shows minor folding due to diagenetic effects associated with compaction.

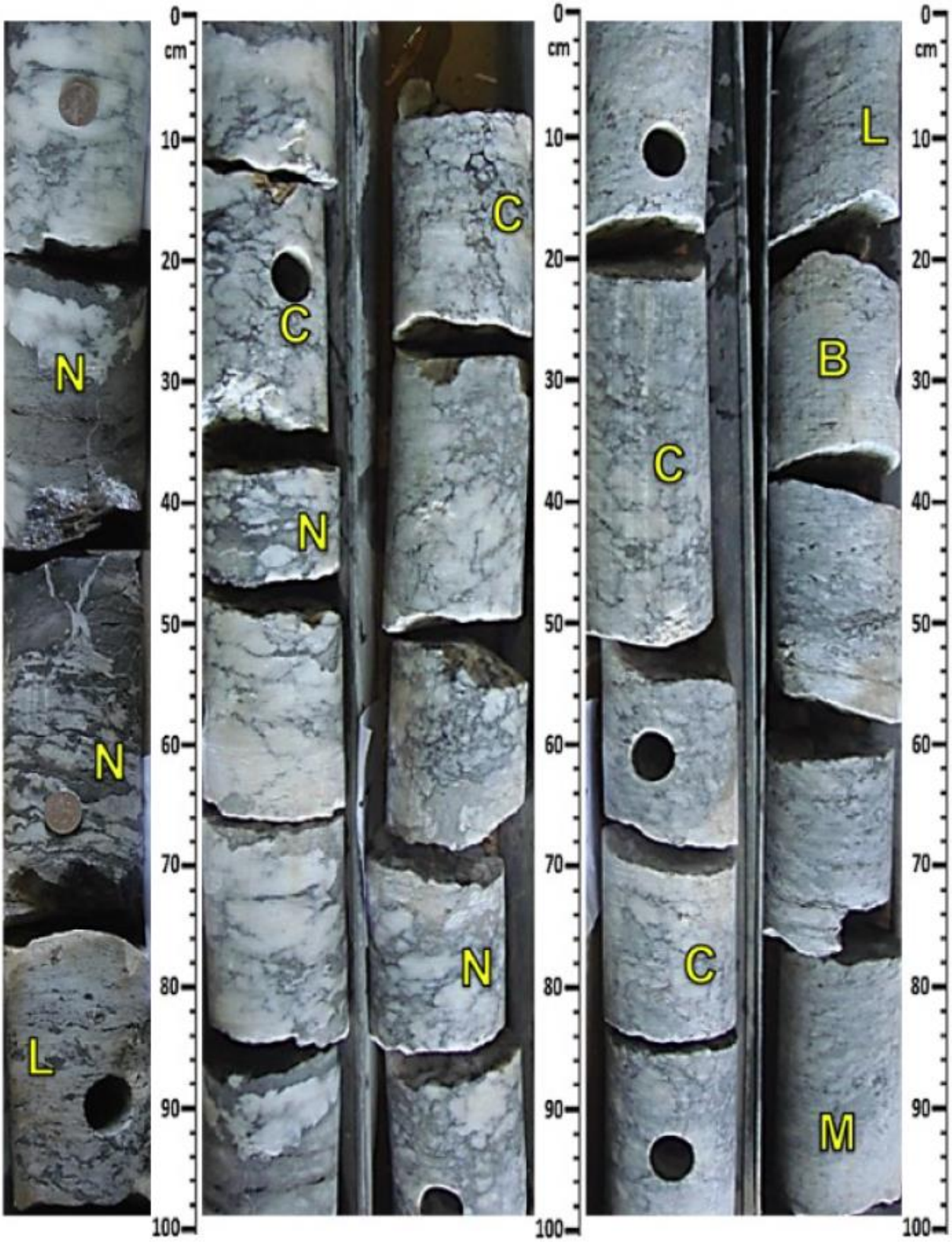

Figure 2. The anhydrite structures of the Butmah Formation: N= nodular, C= chicken-wire, L= laminated, B= bedded, M= massive.

4.2.2 Sparse and isolated crystal textures

This texture consists of sub-spherical, lozenge, oval, or fibrous crystals within a dolomicrite groundmass, as shown in Figure 3C. The size of the crystals is from 0.1 to 1 mm.

4.2.3 Acicular and fibrous textures

These textures (Figure 3D and 3E) are composed of acicular or fibrous crystals depending on the ratio of length to width. In each case, the arrangement of crystals varies from location to location, and can be characterised as parallel, sub-parallel, massive or layered. The fibrous crystals have needle-shaped crystals that range in size from 1 mm to 1 μm. This texture is common in all the anhydrite structures discussed in Sub-section 4.1 above.

4.2.4 Equant/mosaic texture

The crystals of this texture are subhedral to anhedral, ranging in size from 0.1 to 1 mm (Figure 3F). This texture is common in the bedded or laminated anhydrite structures.

4.2.5 Lath-shaped texture

This texture consists of elongate subhedral to euhedral crystals. The texture can be subdivided into a variety of sub-textures according to the length/width ratio of the crystals. In this study, the crystals were characterised as bladed (Figure 3G), bacillary (Figure 3H), tabular, and prismatic, with different dimensions ranging from small to very big (0.02-0.2 mm wide and 0.2-1.5 mm long).

4.2.6 Composite texture

This term is used to recognise the presence of two or more associated textures that may be present in different amounts and/or represent a gradational replacement of one style of texture with another. Figure 3I shows a gradual replacement of aphanitic and mosaic textures in the centre of the image with equant and lath shape textures on the edges of the image.

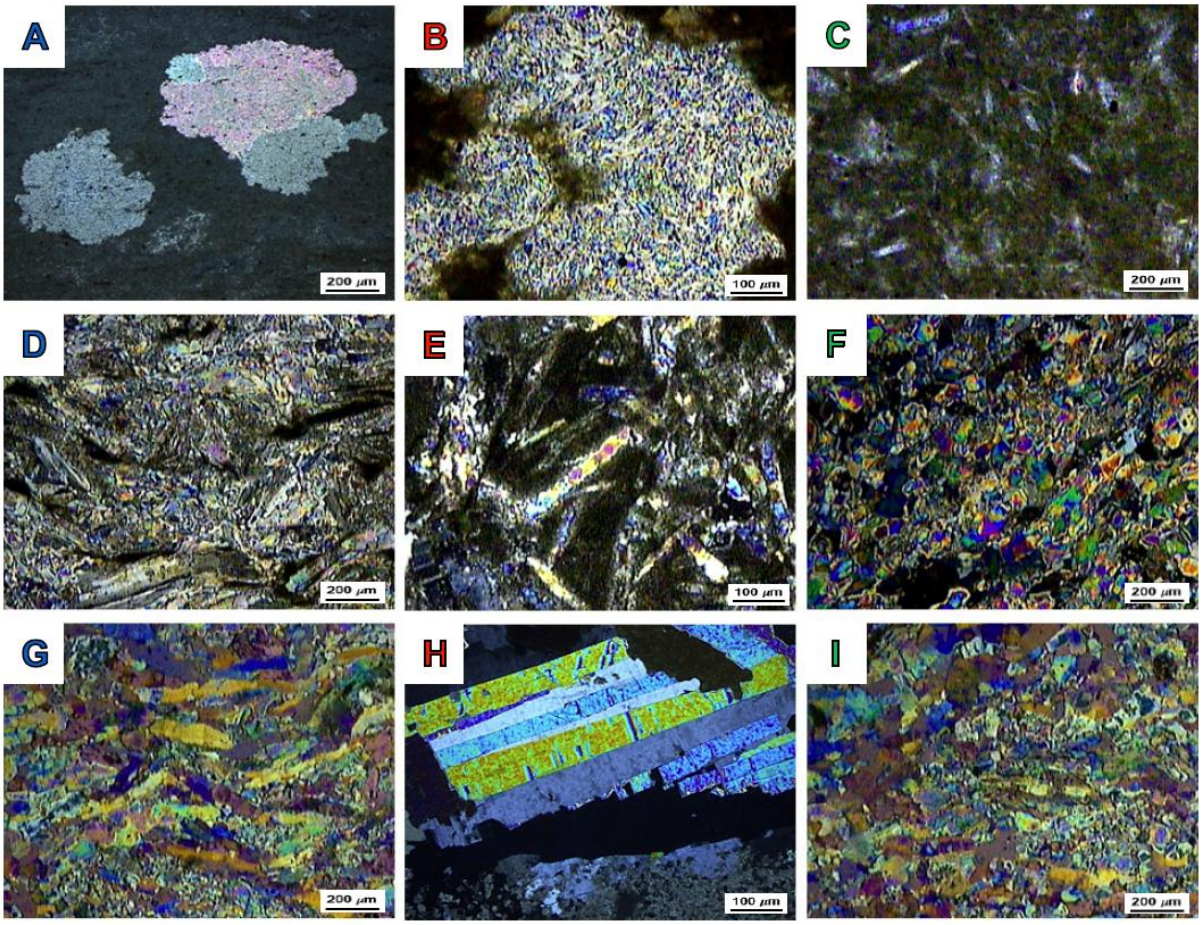

Figure 3. The anhydrite textures of the Butmah Formation. (A) Aphanitic texture; (B) Felted anhydrite texture; (C) Sparse and isolated crystals in dolomudstone; (D) Acicular anhydrite texture; (E) Fibrous anhydrite texture; (F) Equant/mosaic anhydrite texture; (G) Bladed lath-shaped anhydrite texture; (H) Bacillary lath-shaped anhydrite texture; (I) Composite anhydrite texture.

5. DEPOSITIONAL ENVIRONMENT OF THE BUTMAH FORMATION

The microfacies summarise all the sedimentological and palaeontological criteria that can be studied in thin sections (Flügel, 2010). The depositional system controls the vertical and lateral microfacies distribution by sea-level change, salinity, temperature, light penetration, water depth, energy, and turbidity (Miall, 1984). In this work, microfacies were characterised by microscopical study of thin section slides of the cored intervals and of cuttings samples from the studied wells. Eight microfacies were identified based on sedimentological, petrographic and palaeontological investigations in the carbonates and anhydrites of the Butmah Formation and are summarised in Table 1 and Figure 4.

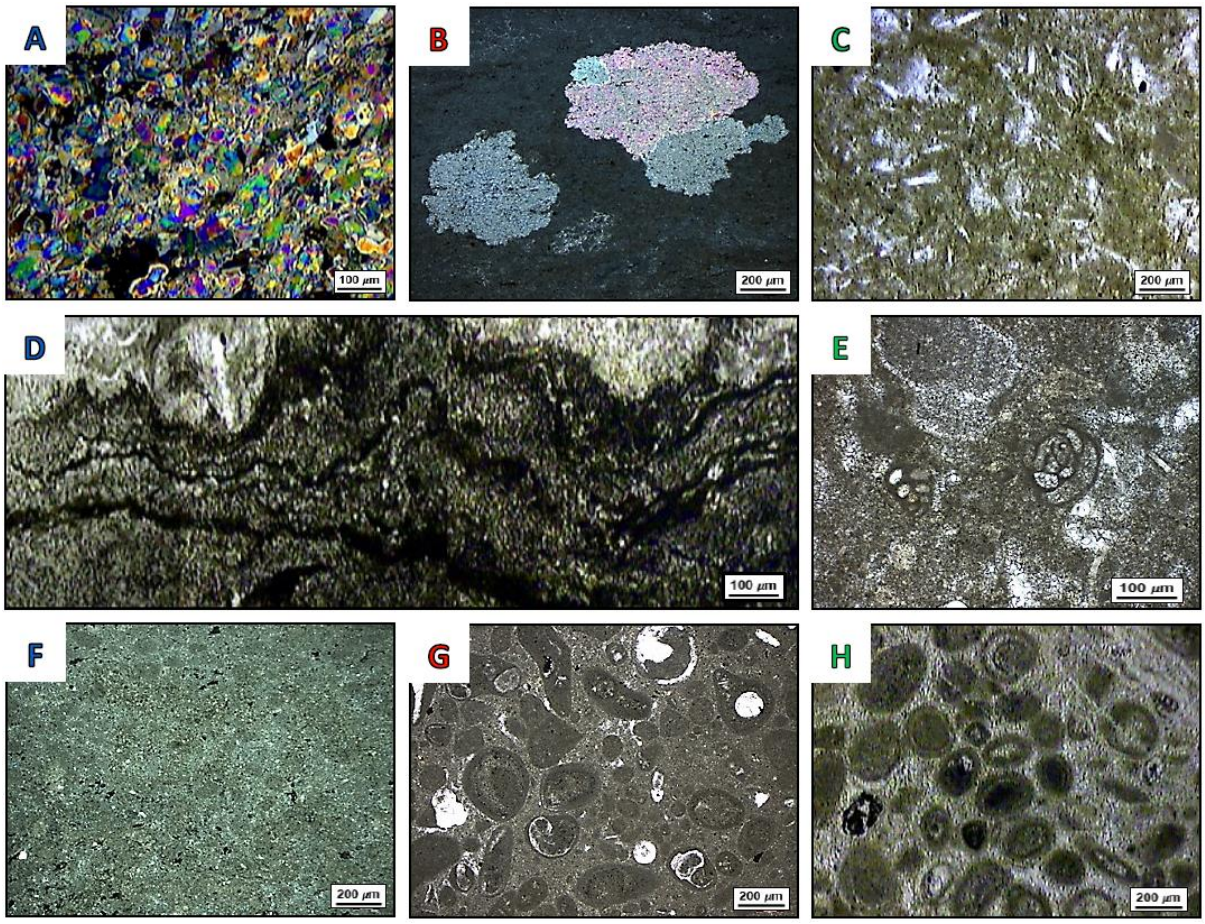

Figure 4. The eight microfacies recognised in the Butmah Formation. (A) Crystalline anhydrite microfacies (granular texture), Bm-15, (2340 m); (B) Nodular dolomudstone microfacies, Bm-15, (2500 m); (C) Dolomudstone with sparse anhydrite microfacies, Bm-15, (2350 m); (D) Stromatolite boundstone, Bm-15, (2378 m); (E) Fossiliferous packestone microfacies showing Foraminifera (Miliolids & Textularia), Bm-15, (2280 m); (F) Peloidal wackstone/packstone, Bm-15, (2541 m); (G) Peliodal-ooid packstone showing different kinds of ooids, Bm-15, (2627 m); (H) Ooid grainstone, Az-29, (2370 m).

Three major sub-environments are recognised in the Butmah Formation. These are (i) tidal flat (Sabkha, intertidal), (ii) back shoal (Lagoonal), and (iii) shoal sub-environments, all of which are represented in Figure 5.

The tidal flat environment consists of three microfacies, including crystalline anhydrite (B.1), nodular dolomudstone (B.2), and dolomudstone with sparse anhydrite crystals (B.3). The calcareous or dolomitic mudstones include nodular, wavy or coarse crystalline anhydrite with few indigenous biota except for cyanobacteria, ostracods, and those molluscs which are adapted to high salinities. The lagoon environment is represented by four microfacies:

dolomudstone with sparse anhydrite crystals (B.3), stromatolite boundstone (B.4), fossiliferous packstone (B.5), and peloidal wackestone/packstone (B.6). The common biota includes large bivalves, gastropods, and miliolids. The shoal environment is represented by peloidal-ooid packstones (B.7) and ooid grainstones (B.8). This environment consists of peloids and/or ooides with some bioclasts such as gastropod and miliolids, and has been interpreted as medium to high energy (Flügel, 2010). Microfacies B.4 and B.7 occur at the interface between the tidal flat and lagoon environments and between the lagoon and shoal environments, respectively, and may be treated as indicating transitional deposition.

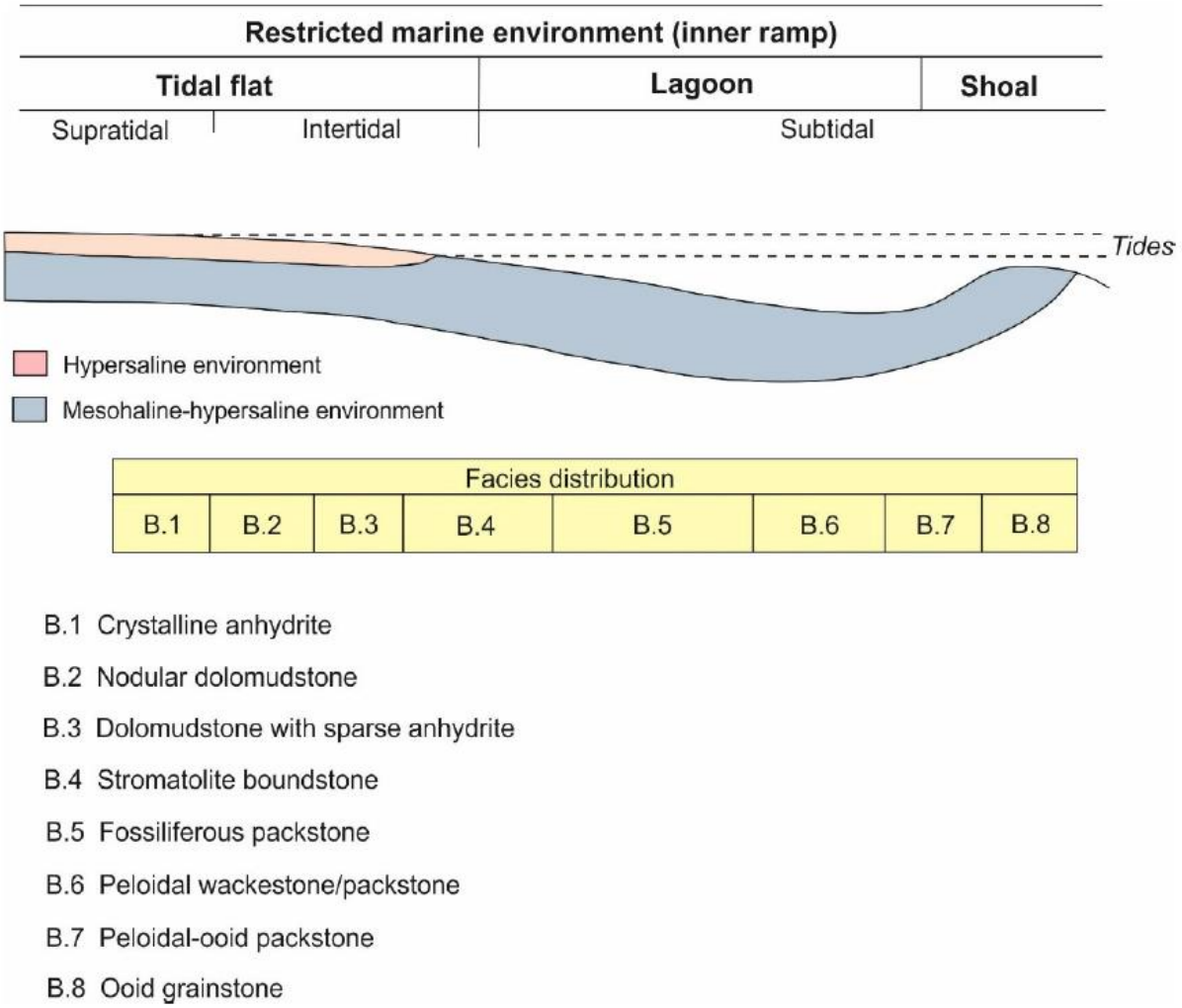

Figure 5. The depositional model with facies distribution of the Butmah Formation (after Jafarian et al., 2018).

Table 1. Summary of the identified microfacies types and depositional environment of the Butmah Formation.

Microfacies	Description	Interpretation	Depositional environment
B.1: Crystalline anhydrite	This microfacies is represented by thin beds of anhydrite which is observed under the microscope as equant, fibrous, felted, and bladed.	It is typical of evaporative low-layers coastline.	Supratidal
B.2: Nodular dolomudstone	This microfacies is composed of laminar or massive dolomudstone and includes differently sized isolated and combined nodules of anhydrite.	It implies tidal flat position, but with fluctuating evaporation rate with shallow depth environment.	Intertidal
B.3: Dolomite with sparse anhydrite	This microfacies is similar to the previous microfacies but with a lesser anhydrite component which is represented as random crystals of anhydrite within a dolomudstone groundmass.	It indicates tidal flat position of carbonate platform with deeper environment than microfacies B.2.	Intertidal
B.4: Stromatolite boundstone	This microfacies is characterised by stromatolite layers which appear under the microscope as frequent dark (micrite) and light (dolospar) algal laminae.	It is typical of a carbonate platform in intertidal and lagoon position.	Transitional Intertidal/Lagoonal
B.5: Fossiliferous packstone	This microfacies consists mainly of miliolid, *Textularia*, gastropods, echinoderms, green algae and peloids.	The common biota of this microfacies indicates lagoon environment (inner platform).	Lagoonal
B.6: Peloidal wackestone /packstone	This microfacies consists of peloids as the main non-skeletal grain associated with some fossils and lithoclasts.	It implies a restricted low energy environment.	Lagoonal
B.7: Peloidal-ooid packstone	This microfacies principally consists of micritic, fibrous ooids and peloids. In addition, intraclasts, shell fragments, benthic foraminifera, and red algae occur.	It implies medium to high energy deposition due to the presence of bioclasts.	Transitional Lagoonal/Shoal
B.8: Ooid grainstone	This microfacies consists mainly of superficial and normal ooids. Furthermore, some peloids, shell fragments, and benthic foraminifera occur within sparry calcite or anhydrite cement.	It is a typical indication for high energy condition with middle platform position.	Shoal

6. PETROPHYSICAL PROPERTIES

This section contains a detailed report of the pore and pore-throat microstructure of the anhydritised carbonate of the Butmah Formation, together with porosity, permeability and other petrophysical parameters related to the reservoir quality of the formation rocks.

6.1 Porosity

Effective porosity values from 67 anydritised samples of limestone and dolomite rocks from units U.4 and U.5 are presented in Table 2 and Figure 6. Overall, the highest porosity in U.4 of the Butmah Formation was 8.6%, and the lowest 0.72%, with an arithmetic mean of 4.62%, a modal value of 3.5%, and a standard deviation of 4.64%. Compared to the Unit U.4 measurements, samples from Unit U.5 showed lower porosities, with a maximum of 6.91%, a minimum of 0.19%, an arithmetic mean of 2.72%, a modal value of 1.5%, and a standard deviation of 3.38%.

Figure 6A shows that the aggregated porosity distribution of the Butmah Formation for units U.4 and U.5 is approximately unimodal, with an arithmetic mean value of 3.67% and a standard deviation of 3.77% overall.

It would be tempting to take the apparent unimodality of the overall distribution at face value. However, when the dataset is separated into limestones and dolomites, as in Figure 6B, it is clear that the overall behaviour is composed of a unimodal distribution for each rock type, with the dolomite samples displaying a higher porosity. The porosity of the limestone samples varies from 0.19% to 6.91%, with an arithmetic mean value of 2.72% and a modal value of 1.5%, while the porosity of the dolomite samples varies from 0.72% to 8.6%, with an arithmetic mean value of 4.62% and a modal value of 3.5%. The dip in the peak of the overall distribution in the range 2%-3% is caused by the addition of the separate distributions for limestone and dolomite.

Table 2. Statistical analysis of the effective porosity of the U.4 and U.5 of the Butmah Formation.

Stratigraphic units	Lithofacies and lithology	Number of samples	Effective porosity (%)				
			Min	Max	Mean	Mode	Std Dev
U.4	L.3 (dolomite)	36	0.72	8.6	4.62	3.5	4.64
U.5	L.1 (limestone)	31	0.19	6.91	2.72	1.5	3.38
Overall	Overall	67	0.19	8.6	3.67	3.5	3.77

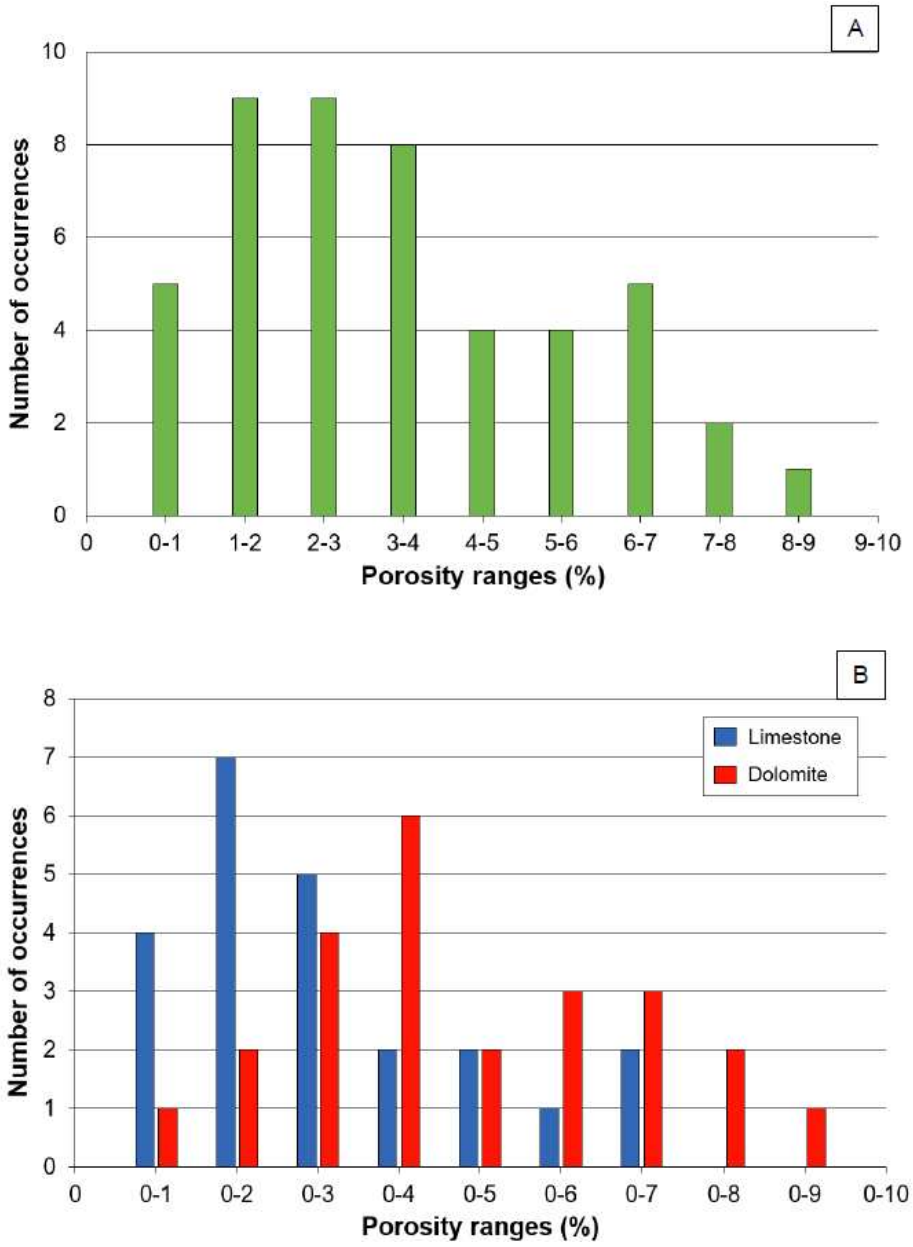

Figure 6. (A) The overall effective porosity of the Butmah Formation; (B) The effective porosity of the Butmah Formation separated into the contributions from the dolomite and limestone lithofacies.

6.2 Pore throat size measurements

The pore-throat size distributions of eight samples of limestone and dolomite from the Butmah Formation were measured using mercury injection capillary pressure analysis, from which the associated pore and grain distributions were also calculated. The measurements show differences in both the pore throat size and pore size distributions between the limestone and dolomite units of the Butmah formation. These differences in the pore microstructure are governed by the dolomite recrystallisation, anhydrite occurrences and subsequent diagenesis (Mohammed Sajed and Glover, 2020). Examples of the measured capillary pressure curves for four samples are given in parts A, C, E and G of Figure 7, while the derived pore throat size distributions are shown in parts B, D, F and H of Figure 7.

The limestone samples exhibit a single peak in the pore throat size distributions, which are shown here as graphs of incremental intrusion as a function of pore throat diameter. The two samples shown in Figure 7 exhibit similar morphology - both of them show moderate pore sorting, with a displacement pressure of 6000 psi in Figure 7A and Figure 7C, respectively, whereas the associated pore throat size distributions shown in Figure 7B and Figure 7D show single peaks at 0.007 µm and 0.03 µm.

By contrast, the dolomite samples exhibit a wide range of pore throat sizes, with displacement pressures of 50 and 80 psi in the two examples shown here (Figure 7E and Figure 7G), and a significant pore volume associate with pore throats from 2 nm to 10 µm, in both cases. These samples both exhibit poor pore throat size sorting, which may be unimodal or multimodal. The pore throat distributions of the two dolomite examples shown in Figure 7F and Figure 7H are clearly different, with one showing significant incremental intrusion between about 0.03 µm and 2 µm, with no clearly dominant peaks, while the other has a single broader peak at approximately 0.8 µm. Clearly, dolomitisation and anhydrite cementation/dissolution have left different parts of this formation with significantly different pore textures based on assessment by pore throat diameter.

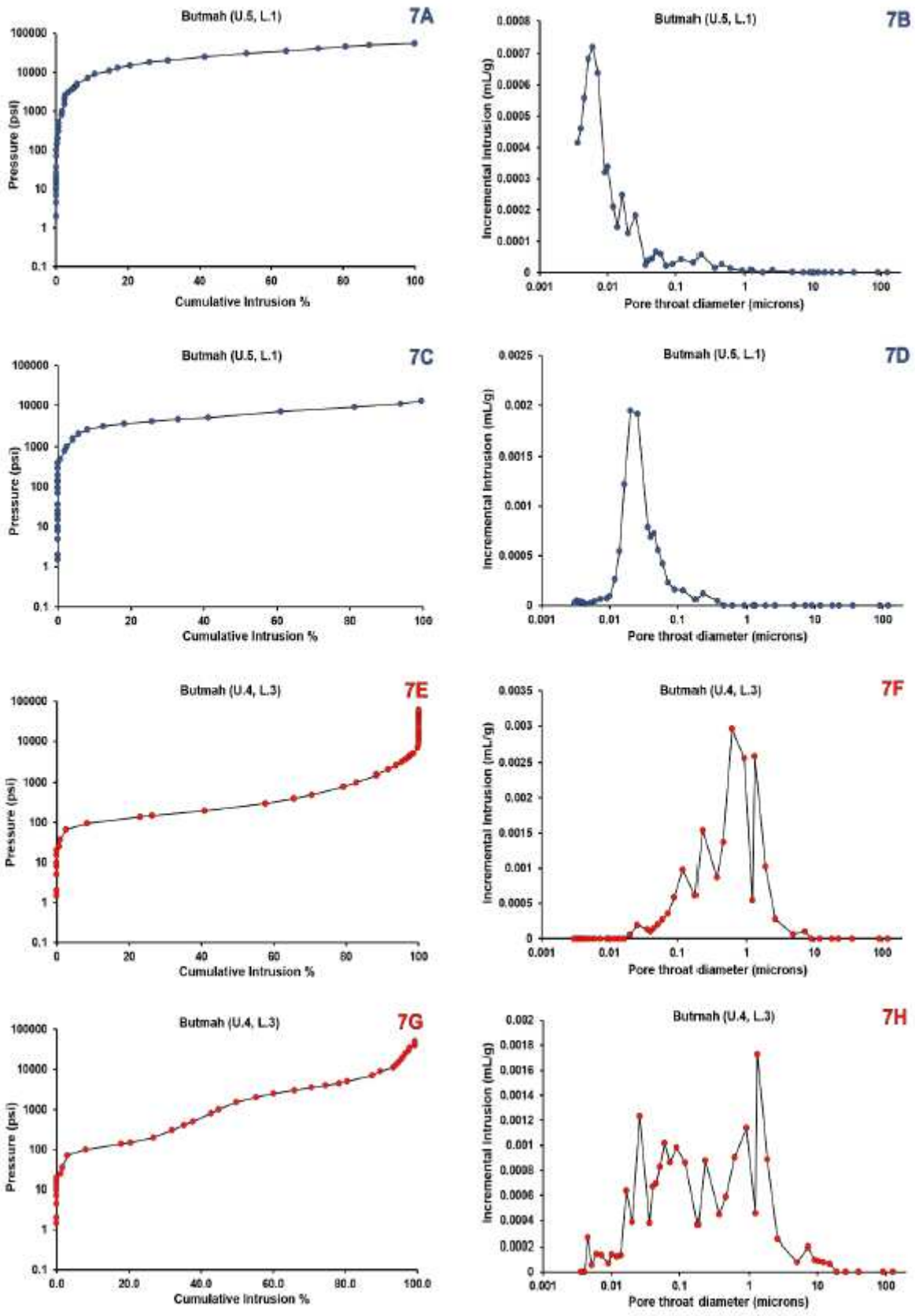

Figure 7. Pore throat distributions for four samples subjected to MICP measurements. Top two rows (blue dots) from the limestone lithofacies (U.5, L.1) of the Butmah Formation, and bottom two rows (red dots) from the dolomite lithofacies (U.4, L.3) of the Butmah Formation.

6.3 Grain/crystal size and pore distributions

In order to get a good description of the pore network of any rock, grain/crystal size, pore size and pore-throat distributions should be identified correctly (Mohammed Sajed and Glover, 2020).

The use of grain/crystal size scales allows more extensive differentiation of limestone and dolomite fabrics. In this study, we used the Folk (1962) classification scheme, as summarised in Table 3.

Table 3. Grain/crystal classification terms according to Folk (1980)

Grain/crystal size classification					
Diameter (μm)	4 - 16	16 - 62	62 - 250	250 - 1000	1000 - 4000
Grain name	Calcilutite		Calcarenite		Calcirudite
	VF, F	M, C	VF, F	M, C	F calcirudite
Crystal name	VF crystalline	F crystalline	M crystalline	C crystalline	VC crystalline

Note: F = fine, VF = very fine, M = medium, and C = coarse, VC = very coarse

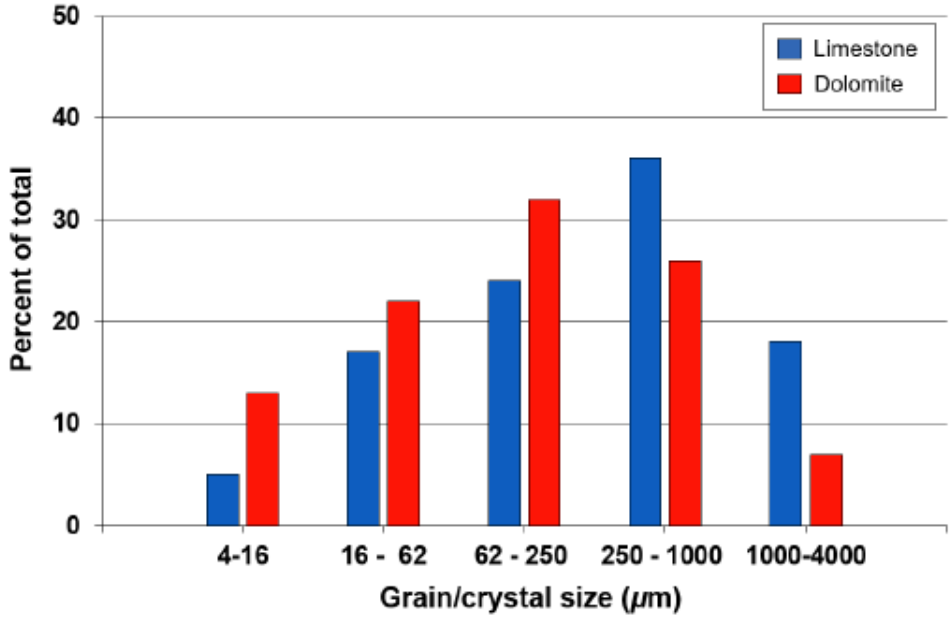

Figure 8. Histogram of grain/crystal size distribution of the limestone and dolomite units of the Butmah Formation using grain and crystal size bins defined by the Folk (1962) classification.

Figure 8 shows grain/crystal size distributions within the Butmah Formation. Wide crystal size distributions were recorded as unimodal histograms for both limestone and dolomite units, ranging from less than 16 µm to more than 1000 µm, with a modal value peaking at 36% in the range 250-1000 µm in the limestones and at 32% in the range 62-250 µm in the dolomites. However, it is clear that the distribution of grain/crystal sizes is approximately the same for the limestone and dolomite-based rock samples studied in this work.

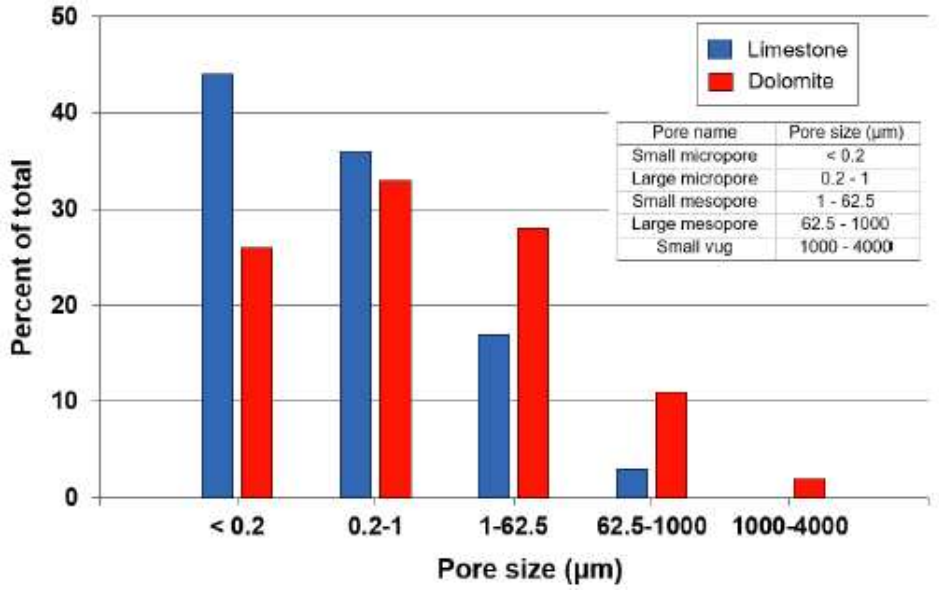

Figure 9. Histogram of the pore size distribution within the Butmah Formation using pore size bins defined by the Luo and Machel (1995) classification.

In this study pore size was also classified using the Luo and Machel (1995) classification. The classification ranges widely from very large pores that can be characterised by the naked eye, and small pores that are measured using polarising microscope, to the very small pores that can be measured by scanning electron microscopy (SEM) and mercury injection capillary pressure (MICP). Figure 9 shows the resulting classified pore size distribution within the Butmah Formation. Overall, it is clear that the smaller sized pores dominate in both the limestones and dolomites. The histogram for the limestone units shows a unimodal pore size distribution ranging from <0.2 to 1000 µm, with a modal pore size of less than 0.2 µm (44% peak value). Whereas the histogram of the dolomite units of the Butmah Formation shows a

pore size distribution range between <0.2 and 4000 µm, exhibiting a modal value in the pore size range of 0.2-1 µm (33% and 34%, respectively).

6.4 Pore network distribution

The pore types occurring in the Butmah formation in this study have been described and classified according to the classification schemes of Choquette and Pray (1970) and Lucia (1983; 1995). In addition, the Ahr (2008) classification has been used to characterise the final shape of the pore network and pore system of the Butmah Formation.

A combination of the previously described petrophysical measurement data and qualitative micrography using both polarising microscopes and SEM has allowed us to characterise the pore network of the studied formation (Table 4).

Table 4: The pore system of the Butmah Formation according to pore type, pore size and grain/crystal size.

Units	Lithofacies & lithology	Grain/crystal size (µm)	Pore type	Pore size (µm)	Pore system
U.4	L.3 (Dolomite)	<16 - >1000	Vg, Inc, Mf	<0.2 – 4000	D & H (d-f)
U.5	L.1 (Limestone)	16 - >1000	Vg, Ing,M, Mf	<0.2 – 1000	H (d-f)

Notes: Vg=vugs, Inc=intercrystalline, Mf= microfractures, Ing= intergranular, M= moldic , D=diagenetic system, H (d-f)=hybrid (diagenetic-fracturing) system.

The limestone units of the Butmah Formation (units 1, 3 and 5) consist of vugs (Vg), intergranular (Ing), moldic (M), and microfractures (Mf) (Figure 10A-C). Generally, there are fewer and smaller pores in these limestones compared to the nearby dolomites (units 1, 3 and 5). Most of the pores are micropores (<2 μm - 62.5 μm). The smaller pores are represented by intergrain spaces, which are mostly isolated pores (Figure 10A). On the other hand, the largest pores are in the form of vugs and molds that are occasionally connected by microfractures or stylolites (Figure 10B), shown by the blue-dyed epoxy with which they are injected, and as partly or totally anhydrite filled pores that can be recognised as white, uniformly-filled patches on the micrographs.

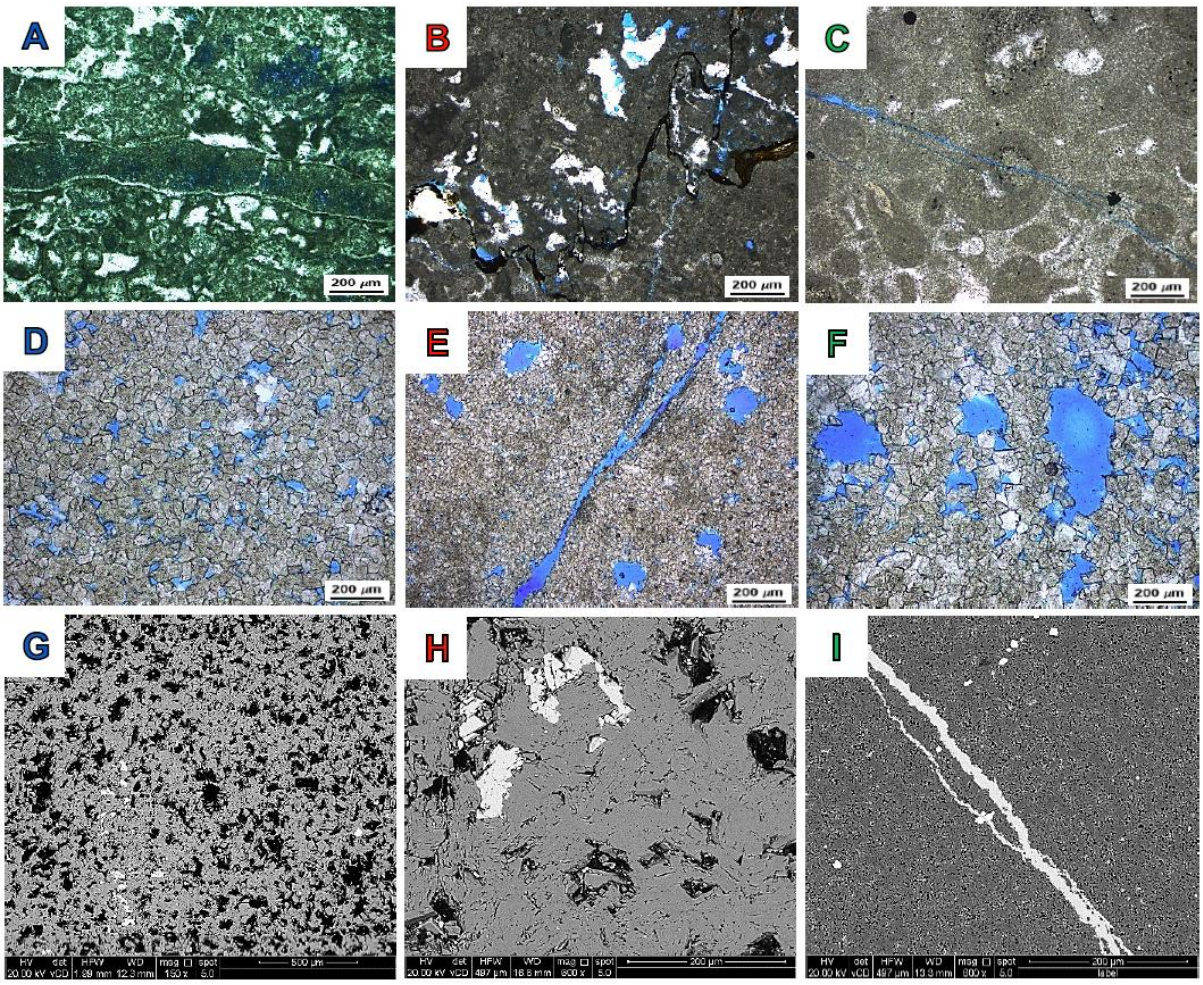

Figure 10. (A) intraparticle and interparticle porosity within limestone facies, U.5, Bm-15; (B) Vuggy porosity associated with stylolite in limestone lithofacies, U.5, Bm-15; (C) Fracture porosity within limestone lithofacies, U.5, Bm-15; (D) Intercrystalline porosity within dolomite lithofacies, U.4, Bm-15; (E) Fracture and isolated vugs in dolomite lithofacies, U.4; (F) intercrystalline porosity with mega vugs within dolomite lithofacies, U.4, Bm-15; (G) SEM image showing intercrystalline porosity partly occluded by anhydrite cement, U.4, Bm-15; (H) SEM image of isolated vugs partly filled by anhydrite cement U.4, Az-29; (I) SEM image of intercrystalline porosity with fractures occluded by anhydrite cement, U.4, Az-29.

By contrast, the dolomite units of the Butmah Formation (units 2 and 4) consist of vugs (Vg), intercrystalline (Inc), and microfractures (Mf) (Figure 10E, F, G). These pores depend on dolomite crystallisation and occurrence of anhydrite cement between the dolomite crystals. This lithofacies has a good porosity when the anhydrite cement is diagenetically dissolved, exhibiting a variety of pore sizes from large mesopores (62.5 μm – 1 mm) to small micropores (<2 μm). The smaller pores are in the form of intercrystalline spaces, which are generally well-

connected (Figure 10D, G). By contrast, the larger ones are often in the form of isolated vugs that may occasionally be connected (Figure 10E, H). Some of these vugs are larger than 0.5 mm, and can be seen as open macropores in Figure 10F.

The fracture intensity in the stratigraphic units of the Butmah Formation is generally high, but most of the fractures have been entirely or partially occluded by anhydrite cement and sometimes by calcite cement. In spite of that, some open fractures were observed, especially in Unit 4 (Figure 10C, E, I).

6.5 Permeability

In general, permeability measurements obtained by core analysis usually represent the lower limit of permeability, especially in fractured units, because core plugs are always chosen from non fractured well-indurated rocks to obtain a whole sample and this leads to a systematic underestimation of permeability (Mohammed Sajed and Glover, 2020).

In this study, permeability measurements were carried out by a pulse-decay method using helium gas permeametery. Summary results are given in Table 5 and Figure 11.

Table 5. Permeability measurements of the studied formations.

Units	Lithofacies & lithology	Number of samples measured	Matrix permeability (mD)			
			Min	Max	Mean	Mode
U.4	L.3 (dolomite)	36	5.41×10^{-5}	6.10×10^{-2}	7.07×10^{-3}	5.0×10^{-4}
U.5	L.1 (limestone)	31	1.30×10^{-6}	7.69×10^{-3}	4.68×10^{-4}	5.0×10^{-5}

The permeability measurements of the anhydrite-containing dolomite rocks composing U.4 of the Butmah Formation show a unimodal distribution, with the lowest permeability being 5.41×10^{-5} mD (5.34×10^{-20} m^2) and the highest being 6.10×10^{-2} mD (6.02×10^{-17} m^2), with an arithmetic mean of 7.07×10^{-3} mD (6.98×10^{-18} m^2), and a modal value of 5.0×10^{-4} mD (4.93×10^{-19} m^2). By contrast, the anhydritised limestone rocks of U.5 show lower permeabilities. They exhibit an unimodal distribution over the range 1.30×10^{-6} mD (1.28×10^{-21} m^2) to 7.69×10^{-3} mD

(7.59×10^{-18} m^2), with an arithmetic mean of 4.68×10^{-4} mD (4.62×10^{-19} m^2), and a modal value of 5.0×10^{-5} mD (4.93×10^{-20} m^2).

Figure 11 shows the permeability distribution on a decadal scale. The permeability of the anhydrite-containing dolomite rocks composing Unit U.4 of the Butmah Formation is distributed predominantly between 0.1 mD and 10^{-5} mD (9.87×10^{-17} m^2 and 9.87×10^{-21} m^2), with the highest occurrence (33.3% of the measurements) in the range 10^{-3} mD – 10^{-4} mD (9.87×10^{-19} m^2 and 9.87×10^{-20} m^2). By contrast, the permeability measurements of the anhydritised limestones of Unit U.5 have a tighter unimodal distribution, with the modal value (48.4% of the measurements) occurring in the range 10^{-4} mD – 10^{-5} mD (9.87×10^{-20} m^2 and 9.87×10^{-21} m^2).

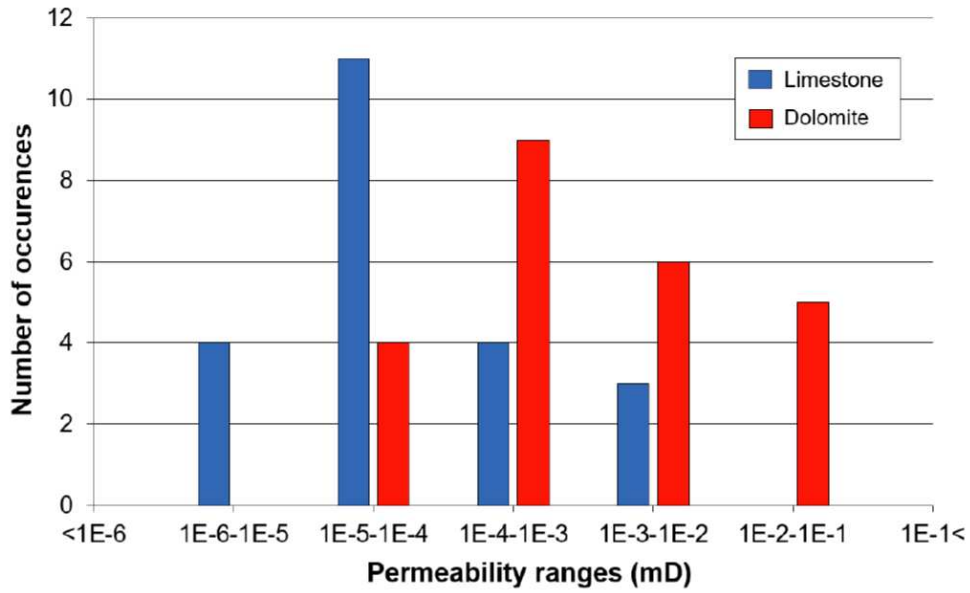

Figure 11. Permeability histogram of the Butmah Formation at well Bm-15.

7. DISCUSSION

Evaporites are usually associated with carbonate dolomitisation as products of the evaporation of seawater or due to the dissolution of sulfate (Melim and Scholle, 2002; Qing et al., 2001). One of the two main mechanisms of dolomitisation, which significantly control the reservoir quality of carbonate rocks in the inner platform environments, is generically related

to saline formation fluids during the precipitation or dissolution of evaporates (Gill et al., 1995; Meyers et al., 1997; Feng and Meyers, 1998; El-Tabakh et al., 2004; Mohammed Sajed and Glover, 2020). Evaluation of the effects of anhydrite fabrics on reservoir quality is very important and complex (Aleali et al., 2013). Consequently, the discussion in this paper emphasises the relationship between the anhydrite fabrics, anhydrite diagenesis, and the reservoir quality of the Butmah Formation.

7.1 Paragenesis of anhydrite

Many factors control the sequence of diagenesis in carbonate rocks, such as mineralogy, grain size, texture, nature of pore fluid and climate (Tucker and Wright, 1990; Tucker, 1993; Ahr, 2008; Flügel, 2010). The effect of anhydritisation on reservoir quality varies according to whether they are early or late anhydrite fabrics during the diagenetic history (Mohammed Sajed and Glover, 2020). Consequently, this section aims to determine the timing of the development of anhydrite structures, textures, and anhydrite diagenesis, and their effects on the reservoir quality of the Butmah Formation.

7.1.1 Anhydrite structures

Starting with anhydrite structures, the nodular to chicken-wire anhydrite structures were deposited under syndepositional supratidal (sabkha) conditions (Kasprzyk, 2005). The nodular anhydrite was formed as very early diagenetic displacement and/or replacement processes (Figure 12). The intensity and shape of anhydrite nodules can vary as a result of water salinity of the depositional environment and the later compaction during burial diagenesis (Shearman, 1966; Warren and Kendall 1985; Machel and Burton, 1991; Tucker, 2001; Warren, 2006; Lucia, 2007). The nodular anhydrite is more common with the dolomite lithology in the tidal flat facies and its presence gives the measured samples moderate to low petrophysical properties (porosity and permeability) and has a reverse relationship with the reservoir quality of the Butmah Formation.

The chicken-wire anhydrite structure was formed due to merged nodules pushing aside and displacing the sediments around them to increase the size of the merged nodules and leading to diffused growth. These structures with the laminated/layered (bedded) structures have been characterised as syndepositional anhydrite textures (Warren and Kendall, 1985; Tucker, 2001; Warren, 2006; Lucia, 2007). Bedded anhydrite may be deposited directly as gypsum from brines and changed diagenetically to anhydrite (Kasprzyk and Orti, 1998; Warren, 2006). The chicken-wire and laminated/layered structures show in general low porosity and permeability which reflected negatively on the reservoir quality of the Butmah Formation.

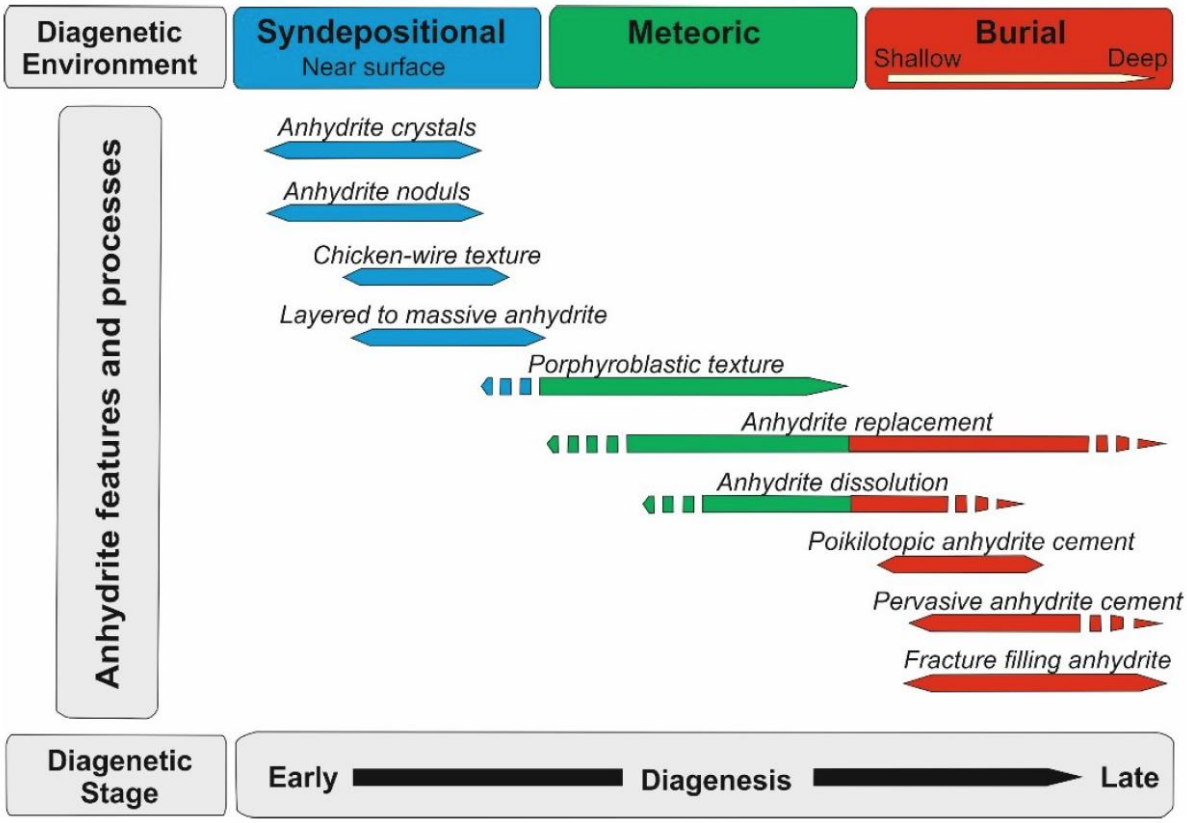

Figure 12. Anhydrite paragenesis of the Butmah Formation.

By contrast, the massive anhydrite structures may belong to the gypsum crystals that formed under subaqueous conditions, then by dehydration (transformation to anhydrite) under deep burial conditions (Logan, 1987; Smoot and Lowenstein, 1991; Warren, 1999). The bedded and

massive structures show very low porosity and permeability and were represented as non-reservoir intervals within the Butmah Formation.

7.1.2 Anhydrite textures

The early anhydrite textures are associated with early dolomitisation and formed in subaerial evaporative conditions or throughout the early diagenetic alteration of the rock (Warren and Kendall, 1984; Kasprzyk, 2003). Under the polarised microscope the early anhydrite structure may exhibit any of the types of anhydrite texture that were described earlier, in Section 4. These textures, which include sparse, aphanitic, felted, acicular, fibrous or mosaic anhydrite textures, reduce the reservoir quality by filling and occluding the host pores within carbonate successions (Mohammed Sajed and Glover 2020).

The so-called sparse and isolated textures represent among the most important syn-depositional textures that are described in the lower zone of the supratidal to the upper zone of the intertidal environments (Warren, 2006; Flügel, 2010; Mohammed Sajed and Glover, 2020). The dispersed and single anhydrite crystals are cut off in some cases by fractures and stylolites, which may have been formed later on through the diagenetic history (Kasprzyk and Orti, 1998). These textures have slightly affected the reservoir quality of the dolomite lithofacies of the Butmah Formation.

The aphanitic and felted textures that are filled with fenestral pores in the dolomite facies of the Butmah Formation belong as well to the early diagenesis that affects the lower zone of the supratidal and the intertidal environments (Warren, 2006; Mohammed Sajed and Glover, 2020). The absence of strong compaction features and stylolites adjacent to the anhydrite cement in the Butmah Formation may refer to their creation during shallow burial. The aphanitic and felted textures have a negative effect on the reservoir quality of the dolomite lithofacies of the Butmah Formation.

The equant/mosaic texture is commonly observed in the tidal flat environments and especially in the shallowest part represented by the supratidal zone (Maiklem et al., 1969; Warren, 2006;

Aleali et al., 2013). The equant/mosaic texture blocked most the pore spaces in the tidal flat facies of the Butmah Formation.

Lath-shaped and composite anhydrite textures are most commonly found in tidal flat and lagoonal facies (Maiklem et al., 1969; Warren, 2006; Aleali et al., 2013). The lath-shaped and composite textures have a clear negative effect on the reservoir quality of the dolomite and limestone lithofacies of the Butmah Formation.

7.1.3 Diagenetic processes

Several diagenetic processes were observed in the Butmah Formation, including anhydrite replacement, anhydrite cementation, anhydrite dehydration, and anhydrite dissolution.

Anhydrite replacement is frequent in the wackestone to grainstone of the lagoon and tidal flat environments of the Butmah Formation. It is a replacement phase, with anhydrite replacing carbonate grains during the percolation of sulfate-rich solutions through the rock. In the Butmah Formation, anhydrite replacement was recognised as occurring not only in grains such as ooides, peliods and bioclasts (Figure 13A, B), but also as commonly affecting the rock mass around fractures (Figure 13C). This process occurs at high temperatures and pressures characteristic of deep burial (Holliday, 1970; Kendall, 1989; Testa and Lugli, 2000).

Anhydrite cementation was characterised mainly into early and late cementation. The early cementation type was previously identified with anhydrite textures that are described as syn-depositional and associated with early diagenetic processes. By contrast, three types of late anhydrite cementation were observed in the Butmah Formation: (i) poikilotopic anhydrite cement, (ii) pervasive anhydrite cement, and (iii) fracture-filling anhydrite cement.

Poikilotopic anhydrite cement is composed of anhydrite crystals of various sizes, arising from matrix dissolution and replaced by anhydrite cement and/or pore-filling (Figure 13D and E). The anhydrite crystals may contain a few carbonate grains or dolomite crystals. The presence of these inclusions is common in the tidal flat, lagoon and shoal environments under deep

burial conditions (Cesaretti et al., 2000; Dworkin and Land, 1994; El-Tabakh et al., 2004). The source of poikilotopic anhydrite cement may be related to dissolution of calcium sulfate under deep burial conditions, or have been formed during early syndepositional brine reflux (Purvis, 1989; Luczaj and Goldstein, 2000; Warren, 2006).

In the Butmah Formation, poikilotopic anhydrite cement reduces the bulk porosity by partially or fully filling interparticle, intercrystalline, and moldic porosity, with a concomitant reduction in permeability. This is contrary to the observations of Lucia (1999), who originally reported that the poikilotopic anhydrite cement only marginally reduced the porosity and permeability of carbonate samples. Moreover, he reported in 2004 that, under some circumstances, poikilotopic anhydrite cement could improve the reservoir quality of carbonate rocks (Lucia, 2004).

Pervasive anhydrite cement consists of contiguous groups of anhydrite crystals that show different extinction angles under the polarised microscope (Figure 13F). This type of anhydrite cement, created due to pervasive large anhydrite crystals, mostly in dolomite facies, is developed pervasively in intergranular/intercrystalline (Ehrenberg et al., 2008; Rahimpour-Bonab et al., 2010). The pervasive anhydrite cement fills pore space in rocks and creates tight carbonate intervals which form a barrier to fluid flow within the reservoirs (Rahimpour-Bonab et al., 2007).

Whereas, the fracture filling anhydrite cement partially or totally fills the Butmah Formation fractures, which leads to reduction of the reservoir quality. The anhydrite crystals in this type tend to be elongated crystals due to the presence of satin-spar gypsum (Kendall, 1975) (Figure 13G and H). Another shape of anhydrite cement was characterised as cemented vugs (Figure 13I).

The poikilotopic and pervasive anhydrite cementation is considered to be a late diagenetic process in the Butmah Formation due to its association with compaction, dissolution, fractures, and saddle dolomite. Finally, fractures filling anhydrite cement were characterised as the latest diagenetic processes in the Butmah Formation.

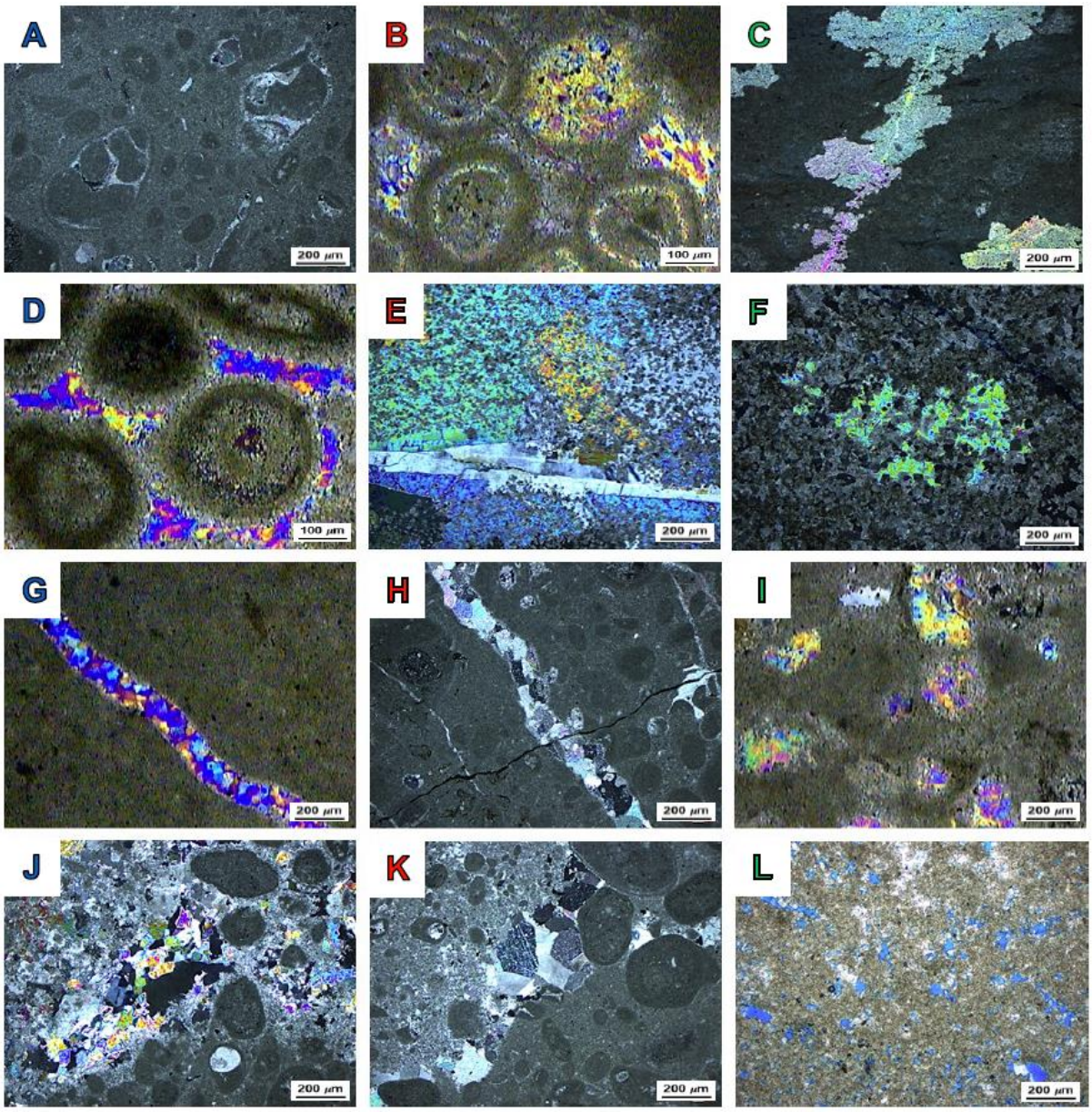

Figure 13. The anhydrite diagenetic features of the Butmah Formation. (A) Anhydrite replacement of a bioclast; (B) Anhydrite replacement of ooids, and matrix; (C) Anhydrite replacement along fracture in dolomudstone; (D) and (E) Pervasive anhydrite cement in ooid grainstone and dolomudstone respectively; (F) Poikilotopic anhydrite cement; (G) Drusy anhydrite cement filling fracture; (H) Multiphase fractures, molds filled by anhydrite cement. New open fracture is cross-cutting the ooid packstone; (I) Anhydrite cement filling vugs; (J) and (K) Anhydrite dehydration as porphyroblastic gypsum; (L) Anhydrite dissolution.

Anhydrite hydration is a type of late diagenetic process in the Butmah Formation that results in secondary gypsum textures such as alabastrine (feathering, granoblastic, and porphyroblastic). It results from uplift or other tectonic activity which allows percolation of

freshwater through calcium sulphate deposits in the meteoric realm (Holliday, 1970; Warren, 1999; 2006) (Figure 13J and K).

The solubility of anhydrite is affected by pressure where each 0.01 Pa increase in pressure results in a steep increase of 3 to 5 times in solubility (Manikhin, 1966). Despite this, water flows through fissures in anhydrite travel for longer distances before sufficient $CaSO_4$ is dissolved to precipitate secondary gypsum than would be the case if the fissures were in massive gypsum (Klimchouk, 1996).

Significant anhydrite dissolution is usually associated with tectonic uplift and exhumation of the platform. The subsequent movement of sulfate-rich brines into deeper and warmer parts of the platform results in precipitation filling pores with anhydrite cement (El-Tabakh et al., 2004).

Dissolution of anhydrite fabrics caused by burial and resulting in high temperatures and pressures may lead to the creation of good reservoir intervals within carbonate succession (Warren, 2006). Such anhydrite dissolution is a late diagenetic process that improves the porosity and permeability of some intervals within the Butmah Formation, giving them good reservoir properties (Figure 13L). The anhydrite dissolution in the Butmah Formation may have coincided with late Jurassic tectonic uplift to improve the reservoir quality of the tidal flat facies. Dissolution of anhydrite beds and nodules is probably the main source of these anhydrite cements in the lagoon and shoal facies of the Butmah Formation.

7.2 Reservoir quality history of the Butmah Formation

According to the facies distribution, anhydrite cementation, and petrophysical properties of the Butmah Formation, we can conclude that the tidal flat facies have the best reservoir quality when compared to the lagoon and shoal facies. These conclusions contrast with the normal situation that is discussed in many literature studies for the reservoir quality of any carbonate successions from the tidal flat facies to the shoal facies (Lee and Harwood, 1989; McNeil et

al., 1998; Testa and Lugli, 2000; Moore, 2001; Al-Ramadan, 2006; Rahimpour-Bonab et al., 2010; Becker et al., 2019).

In general, the precursor pore spaces in the tidal flat facies group tend to be filled partly or totally by the associated syndepositional and early diagenetic anhydrite cement (Phase I). Whereas, in the shoal facies the pore spaces are usually characterised as open with low cement contents due to the high energy of waves at the depositional time. Consequently, the reservoir quality in the shoal and lagoon facies of the Butmah Formation was better than in the tidal flat at the time of the deposition and later in the early diagenetic environments.

The reservoir quality of the Butmah Formation suggests that post-depositional uplift as a tectonic event affected the study area during the Middle-Late Jurassic and caused a contrasting scenario for reservoir facies distribution. The assumed tectonic uplift tended to dissolve some of the early anhydrite cement in the tidal flat facies, and then movement of sulfate-rich brines into the deeper part of the inner platform represented by the lagoon and shoal facies led to saturation and deposition as late anhydrite cementation (Phase II).

The late anhydrite cementation affected enormously the reservoir quality of the lagoon and shoal facies by filling and occluding most of the pore spaces and fractures (Figure 14). Consequently, the tidal flat facies groups have held better reservoir properties than the lagoon and shoal facies groups.

Consequently, we recognise three main stages related to anhydrite cementation which have affected the reservoir quality of the Butmah Formation:

Stage 1 (early diagenetic anhydrite cementation)

The first stage has a negative effect on the reservoir quality of the studied formation and is represented by the amount of anhydrite cement (Phase I) at the depositional time and early diagenetic phase that decreases from the tidal flat facies towards the shoal facies.

Stage 2 (late diagenetic anhydrite dissolution)

This stage mainly occurs due to the late dissolution that dissolves the anhydrite cement in the tidal flat facies and then transports sulfate-rich brines into deeper parts of the inner platform. This stage is responsible for the reservoir quality improvement in the tidal flat facies of the Butmah Formation.

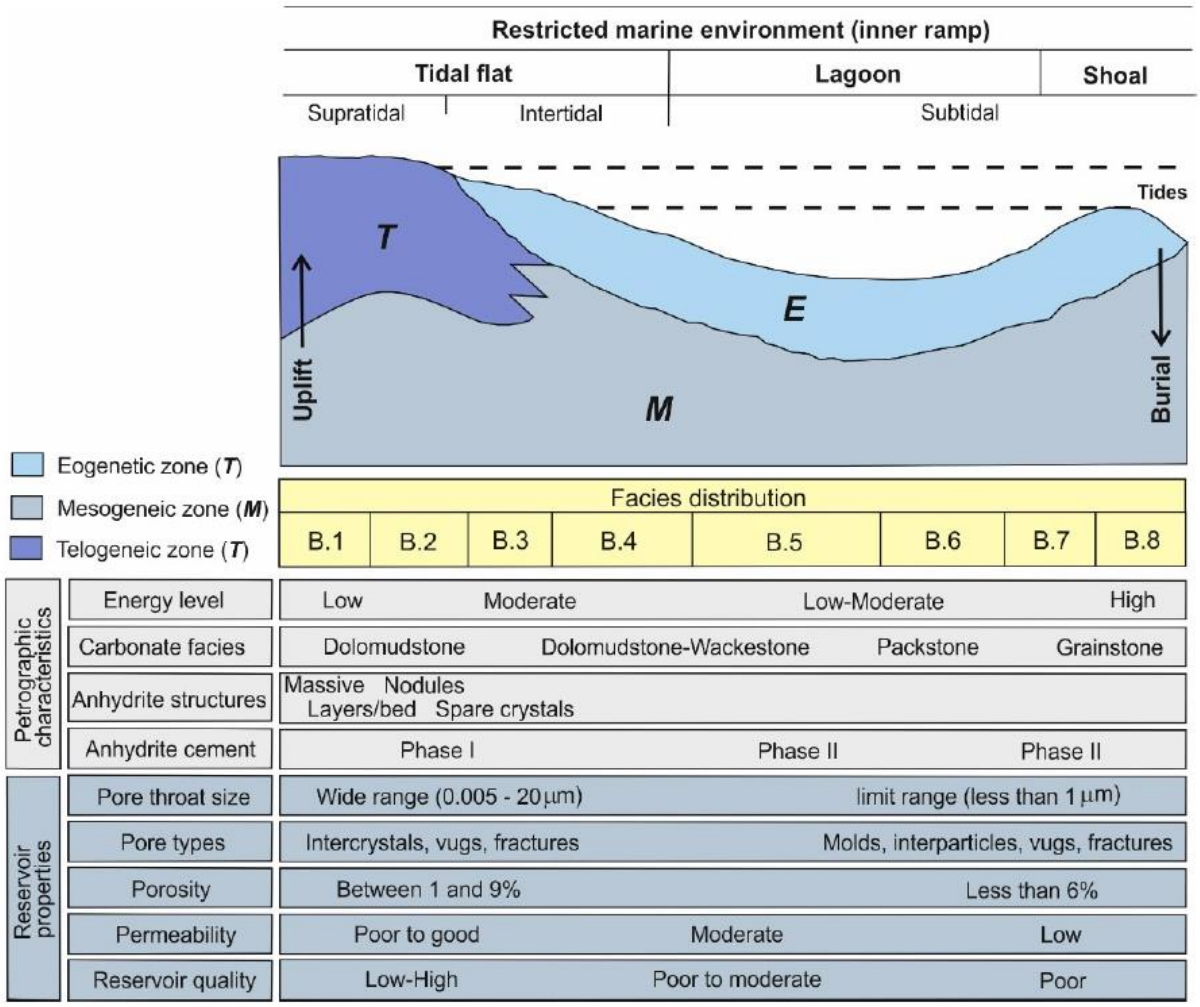

Figure 14. A schematic diagram showing depositional setting, petrographic characteristics, and reservoir properties of the Butmah Formation.

Stage 3 (late anhydrite cementation)

Late dissolution, which affects the tidal flat facies in the earlier stage (Stage 2), led to enrichment of the lagoon and shoal facies by the transported sulfate-rich brines, followed by

deposition as late anhydrite cement (Phase II) to occlude most of the pore spaces and reduce the reservoir quality in the lagoon and shoal facies of the Butmah Formation.

7.3 Anhydritisation and poroperm relationship

This study has shown a clear relationship between anhydrite cementation and the reservoir quality of the Butmah Formation. The massive and bedded anhydrite structures were represented as non-porous and non-permeable intervals within the studied formation (Warren, 1999, 2006, 2010; Aleali et al., 2013).

The lowest reservoir quality in the Butmah Formation was recognised in the lagoon and shoal facies samples that were sharply affected by the late anhydrite cementation (poikilotopic, pervasive and fracture filling anhydrite cement) that gave rise to low porosity, permeability and pore throat.

Deposits of nodular and chicken wire anhydrite are associated with tidal flat and lagoon facies as dolomudstone and dolowackestone and commonly consist of microcrystalline subhedral to anhedral dolomite that is characterised as having moderate reservoir quality with low to moderate porosity and permeability due to association with anhydrite textures such as spare crystals, fibrous, felted and equant textures.

The late diagenetic phase plays two contrasting roles in determining the reservoir quality of the Butmah Formation. It has a negative role of reducing the reservoir quality of the lagoon and shoal facies samples that are sharply affected by the late anhydrite cementation (poikilotopic, pervasive and fracture filling anhydrite cement) to give the worst reservoir quality in the Butmah Formation. However, it also has the positive role of improving the reservoir quality of the tidal flat facies by means of the late anhydrite dissolution, thereby giving the best reservoir quality in the Butmah Formation.

Figure 15 shows the poroperm data for all the samples tested in this work. The porosity is plotted on the x-axis on a linear scale, whereas the permeability is plotted on the y-axis using a logarithmic scale, while pore throat diameter is plotted on the right side of the figure.

Together with overlain curves for the RGPZ carbonate model for four different combinations of parameters. Each of these combinations keeps the cementation exponent constant (m=3.06, and 2.6 for dolomite and limestone samples, respectively) due to the tightness of differences in the two lithologies, and varies the grain/crystal size from 10 µm to 300 µm. Applying the RGPZ carbonate model required the calculation of mean cementation exponents and theta (the coefficient proportionality between the pore size and grain size) values (Glover et al., 2006; Rashid et al., 2015a; 2015b).

The cementation exponents of the dolomite samples varying between 3.74 and 2.03 with an arithmetic mean of 3.06 and a standard deviation of 0.44, whereas the cementation exponents of the limestone samples varying between 3.48 and 1.58 with an arithmetic mean of 2.61 and standard deviation of 0.51. The dolomite samples' calculated theta ranged from 0.008 to 0.096 with an arithmetic mean of 0.035 and a standard deviation of 0.022. In contrast, the range of the calculated theta of the limestone samples covers higher values (0.064 to 0.769) with an arithmetic mean of 0.31 and a standard deviation of 0.195.

Increasing the cementation exponent shifts the curves towards lower permeabilities. It is not possible to fit the tight carbonate models to the data without a further constraint, such as knowing the cementation exponent and modal grain/crystal size (Mohammed Sajed and Glover, 2020). However, the overlay curves show that the data approximately conform to reasonable values for the model parameters. The poroperm relationship clearly shows that the limestone and dolomite samples are very diffuse (huge range of porosities for a given permeability). For instance, permeability at $5x10^{-4}$ mD ($4.93x10^{-19}$ m^2) has porosity ranging from 1.5 – 7.0%, and for 3% porosity, permeability ranges over almost 3 orders of permeability magnitude. These two examples illustrate that it is not porosity which has the biggest controlling influence on permeability but the connectivity of the pores.

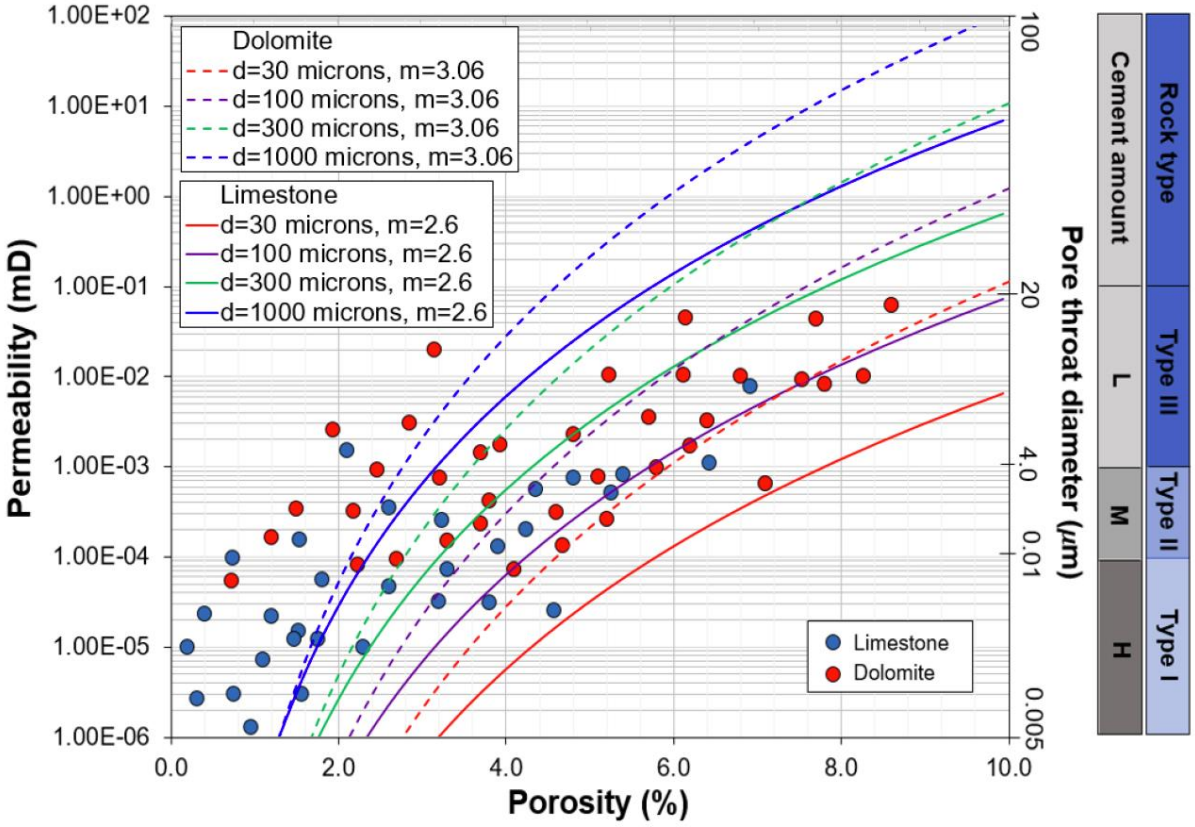

Figure 15. Porosity - permeability relationships of the Butmah Formation showing the distribution of pore-throat diameter and anhydrite cementation amounts.

Consequently, we determined the electrical connectedness values of the selected samples using the following equation from Glover (2009; 2015):

$$G = \phi^m, \quad \textbf{(1)}$$

which should be contrasted with the electrical connectivity, which is given by (Glover, 2009; 2015) by

$$\chi = \phi^{m-1}, \quad \textbf{(2)}$$

where χ is electrical connectivity, G is the electrical connectedness, ϕ is porosity, and m is cementation factor. The two measures differ in that the connectedness describes how the pore network is connected electrically due to the effect of the size of the porosity and the way the pores are connected, whereas connectivity is only concerned with how the pores are

connected. Consequently, heuristically and mathematically, it may be stated that (Glover and Déry, 2010)

$$G = \phi\chi \quad \textbf{(3)}$$

Connectedness is also the inverse of the resistivity formation factor (Glover, 2009).

Figure 16 shows the connectedness-permeability relationship (G-k diagram) and connectivity-permeability relationship (χ-k diagram) that we introduce for the first time in this study to identify the flow units within the limestone and dolomite samples of the Butmah Formation.

In the case of the connectedness-permeability relationship (Figure 16A), we are comparing a measure of the efficacy of electrical flow (connectedness) with a measure of the efficacy of hydraulic flow (permeability) through the same pore network. Limestones tend to exhibit the lower permeabilities, while dolomites have the higher permeabilities. Low permeability rocks of both types tend to have low connectednesses, and for limestones the electrical connectedness changes little while the permeability varies over three orders of magnitude. This implies that as permeability decreases the pore network remains connected electrically, which is consistent from what we know of capillary pressure behavior of rocks with small pore throats. Although some of the tighter dolomites exhibit this same behavior, for permeabilities greater than about 2×10^{-4} mD, the electrical connectedness increases by two orders of magnitude in a scattered manner, indicating that the individual pore microstructures of the dolomite are influencing both the electrical connectedness and the hydraulic permeability.

In the case of the connectivity-permeability relationship (Figure 16B), we are comparing a measure of how the connections of pores affect electrical flow in the rock with the hydraulic permeability. This figure is, perhaps surprisingly, completely different from that in Figure 16A. The electrical connectivity decreases as permeability increases, which is counterintuitive given that both electrical and hydraulic flow depend on the same pore network. Electrical connectivity is more difficult to interpret because it depends directly on both cementation

exponent and porosity (Eq.(2)), but cementation exponent is also dependent on porosity, as we can see for the Butmah Formation in Figure 16C. This results in a complex mathematical relationship which is out of the scope and length of this paper to explore fully.

The apparently diverging relationships shown in Figure 16B makes this figure good for separating rocks according to their properties. Hence we can use the connectivity-permeability relationship to define different flow units. We have divided the limestone and dolomite samples from the Butmah formation samples into three flow units:

1. Flow Unit 1 (χ>3×10^{-3} and k≤1×10^{-5} mD),
2. Flow Unit 2 (10^{-3}<χ<3×10^{-2} and 1×10^{-5}<k<1×10^{-3} mD) , and
3. Flow Unit 3 (10^{-4}<χ<7×10^{-3} and k≥1×10^{-3} mD).

The dolomite samples show the higher permeability values in comparison to the limestone samples and occur solely in flow units 3 and 2. On the other hand, while the limestone samples show the lowest permeability values they occur in all flow units.

Consequently, Figure 17 further shows three types of rock of the Butmah Formation according to all apparent relationships (porosity - permeability - connectivity - anhydrite cement). The porosity is plotted on the x-axis using a linear scale, whereas the permeability is plotted on a logarithmic scale on the y-axis, while the pore throat diameter is plotted on the right side of the relationship. Together with two different direction arrows for electrical connectedness and the degree of anhydrite cementation. Furthermore, this relationship also illustrates the three flow units described in Figure 14.

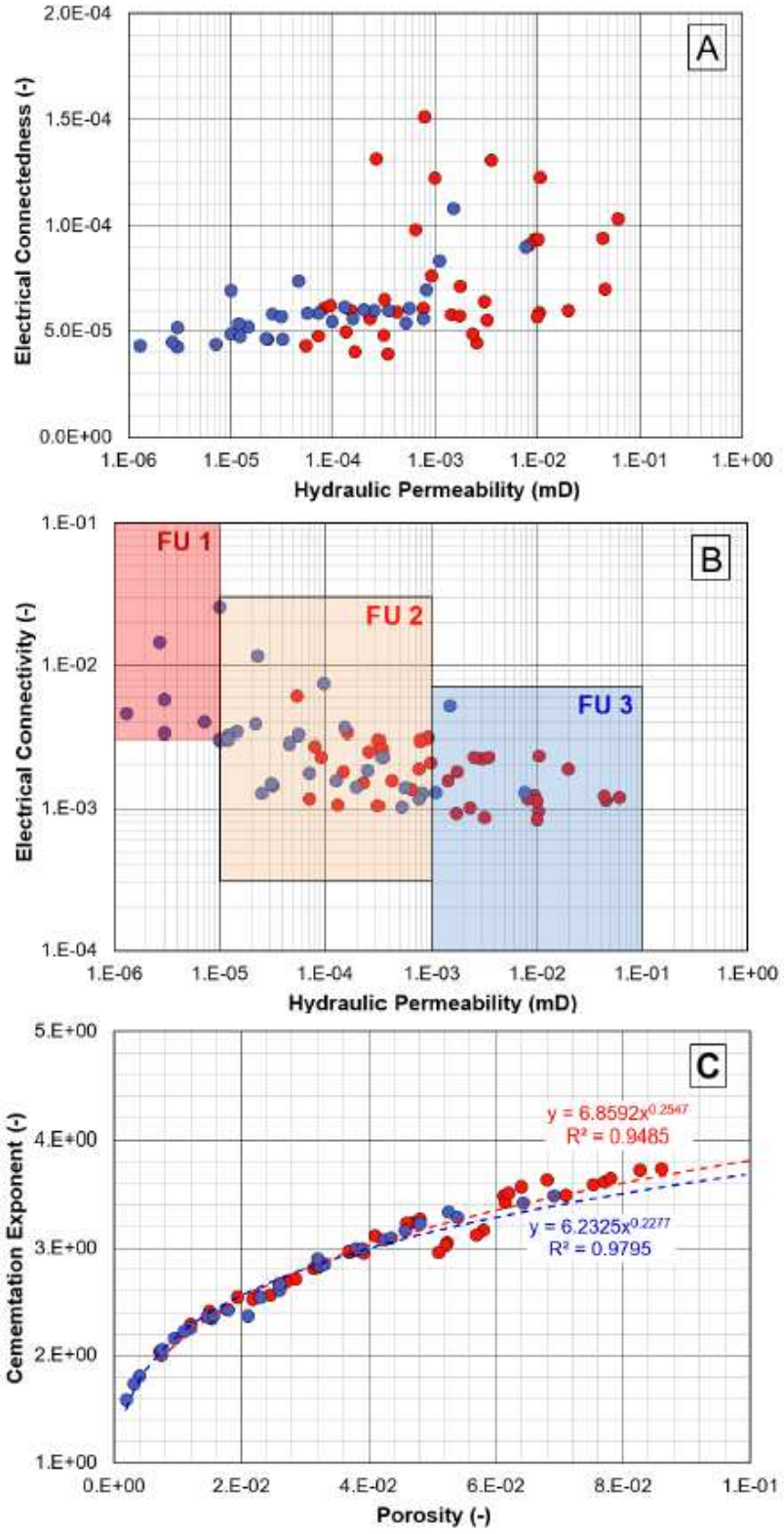

Figure 16. Electrical and hydraulic flow cross-plots. (A) Electrical connectedness (Eq.(1)) as a function of hydraulic permeability. (B) Electrical connectedness as a function of hydraulic permeability, with imposed flow units: FU1 = flow unit 1, FU2= flow unit 2, FU3= flow unit 3. (C) Cementation exponent as a function of porosity with fitted power laws. In each case blue represents limestone and red represents dolomite.

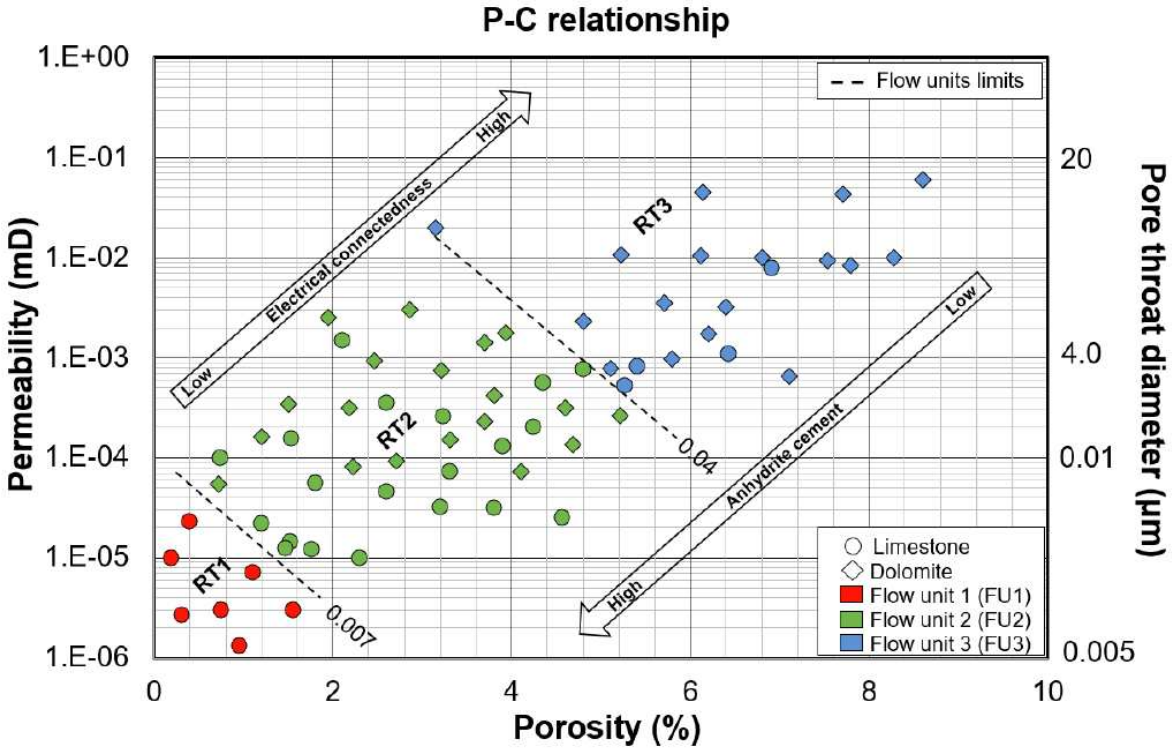

Figure 17. Porosity – permeability – electrical connectedness – cementation relationships of the Butmah Formation showing the three identified rock types; RT1 = Rock Type 1, RT2= Rock Type 2, RT3= Rock Type 3.

Consequently, the porosity-permeability-connectedness-anhydrite relationships described in this work has been used to divide the Butmah Formation into three rock types. These three rock types are described below:

Type I (limestone with high anhydrite cementation):

This rock type is characterised in the Butmah Formation as different kinds of limestone (mudstone, wackestone, packstone, and grainstone). This type has a low porosity, mostly less than 2%, and a permeability $k \leq 1 \times 10^{-5}$ mD, with a pore-throat diameter between 0.005 and 0.01 μm and an electrical connectivity $\chi > 3 \times 10^{-3}$. Pores of this type of rock are represented by some biomolds, fractures and intercrystalline pores that are sharply affected by late anhydrite cementation. Late anhydrite cements (Phase II) were characterised in this type by

such as poikilotopic, pervasive and fracture filling anhydrite cements that occluded most of the pore spaces and reduced the reservoir quality of the lagoon and shoal facies.

Type II (limestone/fine or very coarse crystalline dolomite with moderate anhydrite cementation):

This rock type consists mainly of limestone (wackestone, packstone, and grainstone) and fine or very coarse dolomite crystals. The porosity of this type ranges from low to moderate, mostly less than 6%, with a permeability range $1\times10^{-5}<k<1\times10^{-3}$ mD, pore-throat diameter between 0.007 and 5 μm, and electrical connectivity $10^{-3}<\chi<3\times10^{-2}$. This type of rock has pores such as isolated and/or connected vugs, intercrystalline and microfractures with moderate effect of anhydrite cementation. Both Phase I and Phase II (early and late) anhydrite cements were described in this rock type and represented by the amount of anhydrite cement (Phase I) at the depositional time and early diagenetic phase that decreased from the tidal flat facies towards the lagoon facies and in Phase II mainly in the shoal facies that reduced towards the lagoon and shoal facies.

Type III (medium to coarse crystalline dolomite/fractured limestone with low anhydrite cementation):

This rock type is identified in the studied formation as having moderate porosity of less than 9%, together with a permeability range $k\geq1\times10^{-3}$ mD , a pore-throat diameter between 5 and 10 μm, and an electrical connectivity $10^{-4}<\chi<7\times10^{-3}$. This type of rock has pores such as isolated and/or connected vugs, intercrystalline and microfractures, with low effect of anhydrite cementation that may have happened due to late dissolution that dissolved most of the early anhydrite cement in the tidal flat facies. Some limestone samples described in this type may have been affected mainly by fracturing and retained some intergranular and moldic pores.

8. CONCLUSIONS

The analyses carried out as part of this study have shown that the reservoir quality of the Butmah Formation was affected considerably by anhydrite cementation through the diagenetic history of the Butmah Formation. The main conclusions are:

- Two phases of anhydrite cementation were recognised in this study: Phase I as early anhydrite cement including all the syndepositional and early anhydrite textures, and Phase II as late anhydrite cement represented by the late diagenetic textures of anhydrite.
- The early anhydrite fabrics are associated with the dolomitisation in the tidal flat facies of the Butmah Formation that reduced the reservoir quality of the Butmah Formation by occluding the early intercrystalline pores of the dolomitised units (U.2 and U.4).
- The late anhydrite cements such as poikilotopic textures have reduced the reservoir quality of the Butmah Formation by occluding most of the previously open pore spaces. This occurs especially in the limestone units (U.1, U.3, and U.5) of the lagoon and shoal environments of the Butmah Formation.
- The late anhydrite dissolution was responsible for creating the best reservoir quality of the Butmah Formation by dissolving most of the early anhydrite cementation and creating new pore spaces (intercrystalline, vuggy, fracture, and channel). These processes have created reservoir intervals within the dolomitised units of the Butmah Formation, especially U.4.
- Early anhydrite cementation, dolomitisation and late dissolution have contributed to create the reservoir quality of the tidal flat facies, dolomitised units (U.2 and U.4) of the Butmah Formation, whereas the late anhydrite cementation is the dominant control on the reservoir quality of the lagoon and shoal facies, limestone units (U.1, U.3, and U.5) of the Butmah Formation.

- According to the relationship between the anhydrite cementation and the petrophysical properties of the Butmah Formation, three rock types were characterised in the Butmah Formation: (i) limestone with high anhydrite cementation, (ii) limestone/fine or very coarse dolomite with moderate anhydrite cementation, and (iii) medium to coarse dolomite/fractured limestone with low anhydrite cementation.

ACKNOWLEDGEMENTS

The authors would like to thank the Geology Department of the North Oil Company (NOC) in Iraq for providing core samples and data.

REFERENCES

Ahmad, M. A., 1997. Sedimentary facies and depositional environments of Jurassic rocks, NW-Iraq. Unpublished, PhD thesis, University of Mosul. 135p.

Ahr, W.M., 2008. Geology of carbonate reservoirs: the identification, description, and characterization of hydrocarbon reservoirs in carbonate rocks. Canada, John Wiley & Sons, Inc., Hoboken, New Jersey, 296 p.

Aleali, M., Rahimpour-Bonab, H., Moussavi-Harami, R., & Jahani, D. 2013. Environmental and sequence stratigraphic implications of anhydrite textures: A case from the Lower Triassic of the Central Persian Gulf. Journal of Asian Earth Sciences, 75, p.110-125.

Al-Ramadan, K., 2006. Impact of Diagenetic Alterations on Reservoir Quality and Heterogeneity of Paralic and Shallow Marine Sandstones.

Alsharhan, A.S. 2006. Sedimentological character and hydrocarbon parameters of the middle Permian to Early Triassic Khuff Formation, United Arab Emirates. GeoArabia, 11, 121–158.

Amel, H., Jafarian, A., Husinec, A., Koeshidayatullah, A., Swennen, R., 2015. Microfacies, depositional environment and diagenetic evolution controls on the reservoir quality of the Permian Upper Dalan Formation, Kish Gas Field, Zagros Basin, Marine and petroleum geology, 67, 57-71.

Aqrawi, A.A., Goff, J.C. , Horbury , A.D. and Saddni, F. 2010. The petroleum geology of Iraq. Scientific Press Ltd, Beacon field, Bucks, 424p.

Asquith, G., and Krygowski, D., 2004. Basic well log analysis. American Association of Petroleum Geologists, Tulsa, Oklahoma, 244 p.

Becker, S., Reuning, L., Amthor, J.E. and Kukla, P.A., 2019. Diagenetic Processes and Reservoir Heterogeneity in Salt-Encased Microbial Carbonate Reservoirs (Late Neoproterozoic, Oman). Geofluids, 2019.

Bellen, R. C. V., Dunnington, H., Wetzel, R. and Morton, D., 1959. Lexique stratigraphique. International, Asie, Iraq, 333p.

Cesaretti, N.N., Parnelly, J., Dominguez, E.A., 2000. Pore fluid evolution within a hydrocarbon reservoir: Yacoraite Formation (Upper Cretaceous), Northwest Basin, Argentina. Journal of Petroleum Geology 23, 375–398.

Choquette, P.W., and Pray, L.C., 1970. Geological Nomenclature and classification of porosity in sedimentary carbonates. American Association of Petroleum Geologists Bulletin, 54, p. 819-834.

Dickson, J.A.D., 1965. A modified staining technique for carbonates in thin section: Nature, 205, p.587-587.

Dunnington, H. V., 1958. Generation, Migration, Accumulation and Dissipation of Oil in Northern Iraq: Middle East, American Association of Petroleum Geologists, special volume, p. 1194-1251.

Dworkin, S.I., Land, L.S., 1994. Petrographic and geochemical constraints on the formation and diagenesis of anhydrite cements, Smackover sandstones, Gulf of Mexico. Journal of Sedimentary Research 64, 339–348.

Ehrenberg, S. N., 2006, Porosity destruction in carbonate platforms. Journal of Petroleum Geology, 29, p. 41-52.

Ehrenberg, S.N., Nadeau, P.H., Aqrawi, A.A.M., 2007. A comparison of Khuff and Arab reservoir potential throughout the Middle East. AAPG Bull. 91 (3), 275-286.

Ehrenberg, S.N., Aqrawi, A.A. and Nadeau, P.H., 2008. An overview of reservoir quality in producing Cretaceous strata of the Middle East. Petroleum Geoscience, 14 (4), p.307-318.

El-Tabakh, M., Mory, A., Schreiber, B.C. and Yasin, R., 2004. Anhydrite Cement after Dolomitezation of Shallow Marine Silurian Carbonate of the Gascoyne Platform, Southern Carnnarvon Basin, Western Australia. Sedimentary Geology , 164, 75-87.

Erdman, N. and Bell, D.C., 2015. Scanning Electron and Ion Microscopy of Nanostructures. In Nanocharacterisation, Royal Society of Chemistry, p. 300-350.

Esrafili-Dizaji, B. and Rahimpour-Bonab, H., 2009. Effects of depositional and diagenetic characteristics on carbonate reservoir quality: a case study from the South Pars gas field in the Persian Gulf. Petroleum Geoscience, 15 (4), p.325-344.

Feng, H.Lu, Meyers, W.J., 1998. Massive dolomitization of a late Miocene carbonate platform: a case of mixed evaporative brines with meteoric water, Nijar, Spain. Sedimentology 45, 263 – 277.

Flügel, E., 2010. Microfacies of carbonate rocks. Verlag Berlin Heidelberg, 984p.

Folk, R.L., 1962. Spectral subdivision of limestone types, p.62-84.

Folk, R.L., 1980. Petrology of sedimentary rocks. Hemphill publishing company, 182p.

Fouad, S. F. A., 2015. Tectonic map of Iraq, scale 1: 1000 000, 3 rd edition, Iraqi Bulletin of Geology and Mining, Papers of the Scientific Geological Conference, 11, p. 1-7.

Giesche, H., 2006. Mercury porosimetery: a general (practical) overview. Part. Part. Syst. Charact. 23, p. 9-19.

Gill, I., Moore, C., Aharon, P., 1995. Evaporitic mixed-water dolomitization on St. Croix, U.S.V.I. J. Sediment. Res., A 65, 591 – 604.

Glover, P., 2009. What is the cementation exponent? A new interpretation. Leading Edge (Tulsa, OK), 28(1), pp. 82-85.

Glover, P.W.J., 2015. Geophysical Properties of the Near Surface Earth: Electrical Properties. Treatise on Geophysics: Second Edition. pp. 89-137.

Glover, P.W.J., Zadjali, I. and Frew, K. 2006. Permeability prediction from MICP and NMR data using an electro-kinetic approach, Geophysics, 71, F49.

Glover, P.W.J. and Walker, E., 2009. Grain-size to effective pore-size transformation derived from electrokinetic theory. Geophysics, 74(1), p. E17-E29.

Glover, P.W.J. and Déry, N., 2010. Streaming potential coupling coefficient of quartz glass bead packs: Dependence on grain diameter, pore size, and pore throat radius. Geophysics, 75(6), p. F225-F241.

Haines T.J., Michie, E.A.H., Neilson, J.E., and Healy, D. 2016. Permeability evolution across carbonate hosted normal fault zones, Marine and Petroleum Geology, 72, p. 62-82.

Hart, E. and J.T.C. Hay, 1974, Structure of Ain Zalah Field, Northern Iraq. AAPG Bulletin, 58(6), p.973-981.

Holliday, D.W., 1970. The Petrology of Secondary Gypsum Rocks: A Review. Jou rnal of Sedimentary Petrology , 40, 734-744.

Jafarian, A., Javanbakht, M., Koeshidayatullah, A., Pimentel, N., Salad Hersi, O., Yahyaei, A. and Beigi, M., 2018. Paleoenvironmental, diagenetic, and eustatic controls on the Permo–Triassic carbonate–evaporite reservoir quality, Upper Dalan and Kangan formations, Lavan Gas Field, Zagros Basin. Geological Journal, 53(4), pp.1442-1457.

Jannot, Y., Lasseux, D., Vizé, G. and Hamon, G. 2007. A detailed analysis of permeability and Klinkenberg coefficient estimation from unsteady-state pulse-decay or draw-down experiments. Paper no. SCA2007-08.

Jassim, S. Z., and Goff J. C., 2006, Phanerozoic development of the Northern Arabian Plate. In: Jassim, S.Z. and Goff, J.C. (eds) Geology of Iraq. Dolin, Prague and Moravian Museum, Brno. p. 30-44.

Jassim, S. Z., Buday, T., Cicha, I., and Prouza, V., 2006. Late Permian-Liassic Megasequence AP6. In: Jassim, S.Z. and Goff, J.C. (eds) Geology of Iraq. Dolin, Prague and Moravian Museum, Brno. p. 104-116.

Jennings, J.B. 1987. Capillary Pressure Techniques: Application to Exploration and Development Geology. AAPG Bulletin, 71, p.1196-1209.

Jones, S.C. 1997. A Technique for Faster Pulse-Decay Permeability Measurements in Tight Rocks. Society of Petroleum Engineers, SPE-28450-PA.

Kasprzyk, A. and Orti, F. (1998) Palegeographic and Burial Controls on Anhydrite Genesis: The Badenian Basin in the Carpthian Fore Deep (Southern Poland, Western Ukarine). Sedimentology, 45, 889-907.

Kasprzyk, A., 2003. Sedimentological and Diagenetic Patterns of Anhydrite Deposits in the Badenian Evaporate Basin of the Carpathian Fore Deep, Southern Poland. Sedimentary Geology, 158, 167-194.

Kasprzyk, A., 2005. Diagenetic Alteration Deposits in the Carpathian Fore Deep Basin, Southern Poland: Process and Their Succession. Geological Quaternary , 49, 305-316.

Katz, A. J. and Thompson, A. H. 1987. Prediction of rock electrical conductivity from mercury injection measurements, Geophysical research, 92, p.599-607.

Kendall, A.C., 1975. Anhydrite replacements of Gypsum (Satin-Spar) veins in the Mississippian Caprocks of Southeastern Saskatchewan. Canadian Journal of Earth Sciences 12, 1190–1195.

Kendall, A.C., 1984. Evaporites. In: Walker, R.G., (Ed.), Facies Models : Geoscience Reprint Series 1, Geological Association of Canada, Newfoundland, p.259-296.

Kendall,A.C., 1989. Brine mixing in the Devonian of western Canada and its possible significance to regional dolomitization. Sedimentary Geology 64, 271–285.

Klimchouk, A., 1996. The dissolution and conversion of gypsum and anhydrite. International Journal of Speleology, 25(3), p.21-36.

Klinkenberg, L.J., 1941. The permeability of porous media to liquids and gases. Drilling and production practice. American Petroleum Institute. Production practice, p. 200-213.

Koehrer, B., Heymann, C., Prousa, F., Aigner, T., 2010. Multiple-scale facies and reservoir quality variations within a dolomite body– outcrop analog study from the Middle Triassic, SW German Basin. Marine and Petroleum Geology 27, 386– 411.

Kopaska-Merkel, D.C. and Amthor, J.E. 1988. Very high pressure mercury porosimetry as a tool in reservoir characterization, Carbonate Evaporite, 3, p.53–63.

Lee, M.R. and Harwood, G.M., 1989. Dolomite calcitization and cement zonation related to uplift of the Raisby Formation (Zechstein carbonate), northeast England. Sedimentary Geology, 65(3-4), pp.285-305.

Logan, B. W., 1987. The MacLeod evaporite basin, Western Australia. Mem. American Association of Petroleum Geologists 44, 140p.

Lucia, F.J., 1983. Petrophysical parameters estimated from visual description of carbonate rocks: a field classification of carbonate pore space. Journal of Petroleum Technology, v. 35, p. 626-637.

Lucia, F.J., 1995. Rock-fabrics/ Petrophysical classification of carbonate pore space for reservoir characterization. American Association of Petroleum Geologists, 79, p. 1275-1300.

Lucia, F.J., Ruppel, S.C., 1996. Characterization of diagenetically altered carbonate reservoirs, South Cowden Grayburg reservoir-West Texas. Society of Petroleum Engineers, Paper SPE 36650, pp. 883–893.

Lucia, F.J., 1999. Carbonate Reservoir Characterization: Springer-Verlag, Berlin.

Lucia, F.J., 2004. Origin and petrophysics of dolostone pore space. Geological Society, London, Special Publications, 235(1), p.141-155.

Lucia,F.J.,Jones,R.H.,Jennings,J.W.,2004. Poikilotopic anhydrite enhances reservoir quality (abs.). American Association of Petroleum Geologists Annual Convention Abstracts 13, A88.

Lucia, F. J., 2007, Carbonate reservoir characterization. Springer-Verlag Berlin Heidelberg, 331p.

Luczaj, J.A.y., Goldstein, R.H., 2000. Diagenesis of the lower Permian Krider Member, Southwest Kansas, USA: fluid-Inclusion, U-Pb, and fission-track evidence for reflux dolomitization during latest Permian time. Journal of Sedimentary Research 70, 762–773.

Luo, P., and Machel, G., 1995. Pore size and pore throat types in a heterogeneous dolostone reservoir; Devonian Grosmon Formation, Western Canada basin. American Association of Petroleum Geologists Bulletin, 79, p. 1698-1720.

Machel, H.G., Burton, E.A., 1991. Burial - diagenetic sabkha - like gypsum and anhydrite nodules. Sedimentary Geology 61, 394–405.

Maiklem, W.R., Bebout, D.G. and Glaister, R.P., 1969. Classification of anhydrite--a practical approach. Bulletin of Canadian Petroleum Geology, 17(2), p.194-233.

Manikhin, V.I., 1966. On the question of solubility of calcium sulphate under high pressures. Geokhimicheskie Materialy, v.13. 193-196. (in Russian).

Maurer, F., Martini, R., Rettori, R., Hillgartner, H., and Cirilli, S., 2009. The geology of Khuff outcrop analogues in the Musandam Peninsula, United Arab Emirates and Oman. GeoArabia, 14, 125-158.

McNeil, B., Shaw, H.F. and Rankin, A.H., 1998. The timing of cementation in the Rotliegend sandstones of the Southern North Sea: A petrological and fluid inclusion study of cements. Journal of Petroleum Geology, 21(3), pp.311-327.

McPhee, C., Reed, J., Zubizarreta ,I .2015. Core Analysis : A best practice guide , first edition, 830p.

Melim, L.A., Scholle, P.A., 2002. Dolomitization of the Capitan Formation forereef facies (Permian, West Texas and New Mexico): seepage reflux revisited. Sedimentology 49, 1207 – 1227.

Meyers, W.J., Lu, F.H., Zackariah, J., 1997. Dolomitization by mixed evaporative brines and freshwater, late Miocene carbonates, Nijar, Spain. J. Sediment. Petrol. 67, 898 – 912.

Miall, A.D., 1984. Principles of Sedimentary Basin Analysis. Springer-Verlag New York Inc., 490p.

Mohammed Sajed, O. K., Glover, P. W. J, 2020. Dolomitisation, cementation and reservoir quality in three Jurassic and Cretaceous carbonate reservoirs in north-western Iraq. Marine and Petroleum Geology, 115, p.104256.

Mohammed Sajed, O.K., Glover, P.W. and Collier, R.E.L., 2021. Reservoir quality estimation using a new ternary diagram approach applied to carbonate formations in north-western Iraq. Journal of Petroleum Science and Engineering, 196, p.108024.

Moore, C. H., 2001. Carbonate reservoirs, porosity evaluation and diagenesis in a stratigraphic sequence framework, Developments in sedimentology, Netherland, 55, 444 p.

Passchier, C.W., and Trouw, R.A.J., 2005, Microtectonics: Berlin, Heidelberg, New York, Springer-Verlag, 366p.

Purvis, K., 1989. Zoned authigenic magnesites in the Rotliegend Lower Permian, southern North Sea. Sedimentary Geology 65, 307–318.

Qing, H., Bosence, D.W.J., Rose, P.F., 2001. Dolomitization by penesaline seawater in early Jurassic peritidal platform carbonates, Gibraltar, western Mediterranian. Sedimentology 48, 153 – 163.

Rahimpour-Bonab, H., Shariatinia, Z., Siemann, M.G., 2007. Role of Rifting in Evaporite Deposition in the Great Kavir Basin, Central Iran. Special Publication of Geological Society of London, Geological Society of London, Sp. Pub. 285, 263–279.

Rahimpour-Bonab, H., Esrafili-Dizaji, B., Tavakoli, V., 2010. Dolomitization and anhydrite in Permo-Triassic carbonatesat the South Pars Gas Filed offshore Iran: controls on reservoir quality. Jourrnal of Petroleum Geology 33, 1–24.

Rashid, F., Glover, P.W.J., Lorinczi, P., Collier, R. and Lawrence, J., 2015. Porosity and permeability of tight carbonate reservoir rocks in the north of Iraq. Journal of Petroleum Science and Engineering, 133, pp. 147-161.

Rashid, F., Glover, P.W.J., Lorinczi, P., Hussein, D., Collier, R. and Lawrence, J., 2015. Permeability prediction in tight carbonate rocks using capillary pressure measurements. Marine and Petroleum Geology, 68, pp. 536-550.

Rashid, F., Glover, P.W.J., Lorinczi, P., Hussein, D. and Lawrence, J.A., 2017. Microstructural controls on reservoir quality in tight oil carbonate reservoir rocks. Journal of Petroleum Science and Engineering, 156, p.814-826.

Rushing, J.A., Newsham, K.E., Lasswel,P.M. l, Cox, J.C., and Blasingame, T.A.2004. Klinkenberg-Corrected Permeability Measurements in Tight Gas Sands: Steady-State.Versus Unsteady-State Techniques. SPE 89867.

Sarg, J.F., 2001. The sequence stratigraphy, sedimentology, and economic importance of evaporite-carbonate transitions: a review. Sedimentary Geology 140, 9–42.

Sen, P. and Goode, P., 1992a. Influence of temperature on electrical conductivity on shaly sands. Geophysics 57: 89–96.

Sen, P. and Goode, P., 1992b. Errata, to: Influence of temperature on electrical conductivity of shaly sands. Geophysics 57: 1658.

Sharland P .R ., Archer R ., Casey D.M., Davies R .B. , Hall S .H., Heward A.P ., Horbury A.D. and Simmons M.D., 2001. The Chrono-Sequence Stratigraphy of the Arabian Plate. GeoArabia Special Publication 2, Gulf petrolink, Bahrain, 371p.

Shearman, D.J., 1966. Origin of marine evaporites by diagenesis. Transactions of the Institute of Mining and Metallurgy 75, 208–215.

Smoot, J.P., Lowenstein, T.K., 1991. Depositional environments of non-marine evaporites. In: Melvin, J.L. (Ed.), Evaporites, Petroleum and Mineral Resources. Developments in Sedimentology 50, pp. 189–347.

Spain, D. R. 1992. Petrophysical evaluation of a slope fan/ basin floor fan complex: cherry canyon formation, Ward County, Texas. AAOG Bulletin, 76, p.805-827.

Tavakoli, V., Rahimpour-Bonab, H. and Esrafili-Dizaji, B., 2011. Diagenetic controlled reservoir quality of south Pars gas field, an integrated approach. Comptes Rendus Geoscience, 343, p. 55- 71.

Testa, G. and Lugli, S., 2000. Gypsum-Anhydrite Transformations in Messinian Evaporates of Central Tuscany (Italy). Sedimentary Geology, 130, 249-268.

Tiab, D., and E.C. Donaldson, 2012. Petrophysics: Theory and practice of measuring reservoir rock and fluid transport properties 3rd edition. Elsevier, 950 p.

Tucker, M. E., V. P. Wright, and J. Dickson, 1990, Carbonate Sedimentology. Blackwell Science Ltd. 480p.

Tucker, M. E., 1991. Sedimentary Petrology, an introduction to the origin of Verlag, Berlin Heidelberg New York, 260p.

Tucker, M.E., 1993. Carbonate diagenesis and sequence stratigraphy. Sedimentology Reviews 1, 51–72.

Tucker, M.E., 2001. Sedimentary Petrology. 3rd Edition, Blackwell, Oxford, 260.

Washburn, E.W. 1921. The Dynamics of Capillary Flow, Physical Review, 17, 273-283.

Warren, J.K., and Kendall, C.G. St.C. 1985. Comparison of marine (subaerial) and salina (subaqueous) evaporites: modem and ancient. American Association of Petroleum Geologists Bulletin, 69, 1013–1023.

Warren, J.K., 1999. Evaporates: Their Evolution and Economics. Blackwell Scientific, Oxford, 438.

Warren, J.K., 2006. Evaporites: Sediments, Resources and Hydrocarbons. Springer Verlag, Brunei, pp.1035.

Warren, J.K., 2010. Evaporites through time: Tectonic, climatic and eustatic controls in marine and nonmarine deposits. Earth-Science Reviews, 98(3-4), pp.217-268.

Zhang, M., Takahashi, M., Morin, R. H. and Esaki, T. 2000. Evaluation and Application of the Transient-Pulse Technique for Determining the Hydraulic Properties of Low-Permeability Rocks – Part 1: Theoretical Evaluation. American Society for Testing and Materials: Geotechnical Testing Journal, p.83-90.